**Title:** Genomic insights into the host specific adaptation of the *Pneumocystis* genus and emergence of the human pathogen *Pneumocystis jirovecii*

**Short title:** *Pneumocystis* fungi adaptation to mammals

**Authors:** Ousmane H. Cissé[1*†], Liang Ma[1*†], John P. Dekker[2,3], Pavel P. Khil[2,3], Jung-Ho Youn[3], Jason M. Brenchley[4], Robert Blair[5], Bapi Pahar[5], Magali Chabé[6], Koen K.A. Van Rompay[7], Rebekah Keesler[7], Antti Sukura[8], Vanessa Hirsch[9], Geetha Kutty[1], Yueqin Liu [1], Peng Li[10], Jie Chen[10], Jun Song[11], Christiane Weissenbacher-Lang[12], Jie Xu[11], Nathan S. Upham[13], Jason E. Stajich[14], Christina A. Cuomo[15], Melanie T. Cushion[16] and Joseph A. Kovacs[1]*

**Affiliations:** [1] Critical Care Medicine Department, NIH Clinical Center, National Institutes of Health, Bethesda, Maryland, USA. [2] Bacterial Pathogenesis and Antimicrobial Resistance Unit, National Institute of Allergy and Infectious Diseases, National Institutes of Health, Bethesda, Maryland, USA. [3] Department of Laboratory Medicine, NIH Clinical Center, National Institutes of Health, Bethesda, Maryland, USA. [4] Laboratory of Viral Diseases, National Institute of Allergy and Infectious Diseases, National Institutes of Health, Bethesda, Maryland, USA. [5] Tulane National Primate Research Center, Tulane University, New Orleans, Louisiana, USA. [6] Univ. Lille, CNRS, Inserm, CHU Lille, Institut Pasteur de Lille, U1019-UMR 9017-CIIL-Centre d'Infection et d'Immunité de Lille, Lille, France. [7] California National Primate Research Center, University of California, Davis, California, USA. [8] Department of Veterinary Pathology,

Faculty of Veterinary Medicine, University of Helsinki, Helsinki, Finland. [9] Laboratory of Molecular Microbiology, National Institute of Allergy and Infectious Disease, National Institutes of Health, Bethesda, Maryland, USA. [10] Department of Respiratory and Critical Care Medicine, the First Affiliated Hospital of Chongqing Medical University, Chongqing, China.[11] Center for Advanced Models for Translational Sciences and Therapeutics, University of Michigan Medical Center, University of Michigan Medical School, Ann Arbor, MI, United States. [12] Institute of Pathology and Forensic Veterinary Medicine, Department of Pathobiology, University of Veterinary Medicine Vienna, Vienna, Austria. [13] Arizona State University, School of Life Sciences, Tempe, Arizona, USA. [14] Department of Microbiology and Plant Pathology and Institute for Integrative Genome Biology, University of California, Riverside, Riverside-California, Riverside, USA.[15] Broad Institute of Harvard and Massachusetts Institute of Technology, Cambridge, Massachusetts, USA.[16] Department of Internal Medicine, College of Medicine, University of Cincinnati, Cincinnati, OH, USA.

[†] These authors contributed equally to this work. [*] Correspondence and requests for materials should be addressed to O.H.C (ousmane.cisse@nih.gov) or L.M (mal3@nih.gov) or J.A.K (jkovacs@nih.gov).

**Abstract:** *Pneumocystis jirovecii*, the fungal agent of human *Pneumocystis* pneumonia, is closely related to macaque *Pneumocystis*. Little is known about other *Pneumocystis* species in distantly related mammals, none of which are capable of establishing infection in humans. The molecular basis of host specificity in *Pneumocystis* remains unknown as experiments are limited due to an inability to culture any species *in vitro*. To explore *Pneumocystis* evolutionary adaptations, we have sequenced the genomes of species infecting macaques, rabbits, dogs and rats and compared them to available genomes of species infecting humans, mice and rats. Complete whole genome sequence data enables analysis and robust phylogeny, identification of important genetic features of the host adaptation, and estimation of speciation timing relative to the rise of their mammalian hosts. Our data reveals novel insights into the evolution of *P. jirovecii*, the sole member of the genus able to infect humans.

58

59 **MAIN TEXT**

60 **Introduction**

61 The evolutionary history of *Pneumocystis jirovecii*, a fungus that causes life-threatening
62 pneumonia in immunosuppressed patients such as those with HIV infection, has been
63 poorly defined. *P. jirovecii* is derived from a much broader group of host-specific
64 parasites that infect all mammals studied to date. Until recently, *P. carinii* and *P. murina*
65 (which infect rats and mice, respectively) were the only other species in this genus for
66 which biological specimens suitable for whole genome sequencing were readily
67 available. Inter-species inoculation studies have found that a given *Pneumocystis* species
68 can only infect a unique mammalian species (*1, 2*). Further, rats are the only mammals
69 known to be coinfected by at least two distinct *Pneumocystis* species (*P. carinii* and *P.*
70 *wakefieldiae*) (*3*). Within the *Pneumocystis* genus, *P. jirovecii* is the only species able to
71 infect and reproduce in humans, although the molecular mechanisms of its host
72 adaptation remain elusive.

73 Previous efforts to reconstruct the evolutionary history of *Pneumocystis* have
74 estimated the origins of the genus at a minimum of 100 million years ago (mya) (*4*).
75 Using a partial transcriptome of *P. macacae*, the *Pneumocystis* species that infects
76 macaques, we recently estimated that *P. jirovecii* diverged from the common ancestor of
77 *P. macacae* around ~62 mya (*5*), which substantially precedes the human-macaque split
78 of ~20 mya ago (*6*). Population bottlenecks in *P. jirovecii* and *P. carinii* at 400,000 and
79 16,000 years ago, respectively (*5*), are also not concordant with population expansions in
80 modern humans (~200,000 y ago (*7*)) and rats (~10,000 y ago (*8*)), which suggests a

81 decoupled coevolution between *Pneumocystis* and their hosts. This was the first evidence
82 that *Pneumocystis* may not be strictly co-evolving with their mammalian hosts as
83 suggested by ribosomal RNA-based maximum phylogenies (*9*). A molecular clock has
84 not been tested in any of these phylogenies. A strict co-evolution hypothesis was further
85 challenged by evidence showing relaxation of the host specificity in *Pneumocystis*
86 infecting rodents (*10, 11*). However, the accuracy of speciation times is limited without
87 the complete genomes of additional species including that of *P. macacae*, the closest
88 living sister species to *P. jirovecii* identified to date.
89 The absence of long-term *in vitro* culture methods or animal models for most
90 *Pneumocystis* species has precluded obtaining sufficient DNA for full genome
91 sequencing and has hindered investigation of the *Pneumocystis* genus. So far, only the
92 genomes of human *P. jirovecii* (*12, 13*), rat *P. carinii* (*13, 14*) and mouse *P. murina*, (*13*)
93 are available. These data have provided important insights into the evolution of this
94 genus, including a substantial genome reduction (*12, 13*), the presence of intron-rich
95 genes possibly contributing to transcriptome complexity, and a significant expansion of a
96 highly polymorphic major surface glycoprotein (*msg*) gene superfamily (*13*), some of
97 which are important for immune evasion. However, the lack of whole genome sequences
98 for many species of this genus (particularly the closely related *P. macacae*) has severely
99 constrained the understanding of the implications of these genome features in
100 *Pneumocystis* evolution and adaptation to hosts.
101 To further explore the evolutionary history of the *Pneumocystis* genus, and
102 explore *P. jirovecii* genetic factors that support its adaptation to humans, we sequenced 2
103 to 6 specimens of four additional species: those that infect macaques (*P. carinii* forma

104 specialis *macacae* hereafter referred to as *P. macacae*), rabbits (*P. oryctolagi*), dogs (*P.*
105 *carinii* f. sp. *canis* hereafter referred to as *P. canis*) and rats (*P. wakefieldiae*). We
106 assembled a single representative, nearly full-length genome for three of the species
107 except in *P. canis*, in which we recovered three distinct genome assemblies that appear to
108 represent two separate species. We reconstructed a robust phylogeny of *Pneumocystis*
109 species, estimated their diversification time, and used comparative genomics to identify
110 unique and shared genomic features. Given that wild mammals may be commonly
111 exposed to different *Pneumocystis* species in nature, there is a possibility of historical
112 gene flow among *Pneumocystis* species that we have evaluated.
113
114 **Results and Discussion**
115 **Direct sequencing of *Pneumocystis*-host mixed samples**
116 We sequenced the genomes of *Pneumocystis* species from infected macaques, rabbits,
117 dogs and rats (see Methods and Supplementary Methods). Specimens originated from
118 immunosuppressed animals as a consequence of simian immunodeficiency virus
119 infection in macaques, corticosteroid treatment (rabbits and rats), or possible congenital
120 immunodeficiencies (dogs). For each species, we sequenced samples from 2–6 animals
121 (Supplementary Tables 1 and 2). These data were used to assemble one high quality
122 consensus, nearly full-length genome assembly for each species except *P. canis* for which
123 we recovered two nearly full-length assemblies and an additional partial assembly from
124 separate samples (denoted as A, Ck1 and Ck2). Post assembly mapping revealed a non-
125 negligible amount of genetic variability among samples, for example the average genome
126 wide single nucleotide polymorphism (SNP) diversity among six *P. macacae* isolates is ~

12%. The genome of *P. macacae* was sequenced using Oxford Nanopore long reads and Illumina short read sequences, whereas the other *Pneumocystis* were sequenced only with Illumina (Supplementary Tables 2 and 3). The new *Pneumocystis* genome assemblies range from 7.3 Mb in *P. wakefieldiae* to 8.2 Mb in *P. macacae.* The *P. macacae* and *P. wakefieldiae* genome assemblies consist of 16 and 17 scaffolds, respectively, both of which are highly contiguous and approach the chromosomal level based on similarities with published karyotypes (*3*, *15*) and/or the presence of *Pneumocystis* telomere repeats (*16*) at the scaffold ends (Supplementary Table 3). The genome assemblies of *P. oryctolagi* and *P. canis* (assemblies A, Ck1 and Ck2) are less contiguous with 38, 33, 78 and 315 scaffolds, respectively. All these assemblies except for the partial assembly of *P. canis* Ck2 have very similar total sizes (7.3 – 8.2 Mb) comparable to previously sequenced genomes of *P. jirovecii*, *P. carinii* and *P. murina*, all of which are at or near chromosomal-level with a size of 7.4 – 8.3 Mb (Supplementary Table 3). The genome assemblies are all AT-rich (~71%) and ~3% encodes DNA transposons and retrotransposons (Supplementary Table 3). We also assembled complete mitochondrial genomes from all species in this study, which are similar in size (21.2 – 24.5 kilobases) to published rodent *Pneumocystis* mitogenomes (24.6 – 26.1 kb) (*17*) but smaller than that of *P. jirovecii* (~35 kb) (*17*) (Supplementary Table 3). *P. macacae* has a circular mitogenome similar to *P. jirovecii* (*17*) whereas all other sequenced species have linear mitogenomes.

150 **Genomic differences among *Pneumocystis* species**

151 To assess the extent of genome structure variations among species, we generated whole
152 genome alignment of all representative genome assemblies. We found high levels of
153 interspecies rearrangements ranging from 10 breakpoints between *P. wakefieldiae* and *P.*
154 *murina* to 142 between *P. jirovecii* and *P. oryctolagi* (Fig. 1; Supplementary Table 4).
155 The vast majority of chromosomal rearrangements were inversions, which, for example
156 accounted for 23 out of 29 breakpoints between *P. jirovecii* and *P. macacae*
157 (Supplementary Table 4). Analysis of aligned raw Nanopore and/or Illumina reads back
158 to the assemblies show no evidence of incorrect contig joins around rearrangement
159 breakpoints. There are clearly less rearrangements among rodent *Pneumocystis* species
160 (*P. wakefieldiae*, *P. carinii* and *P. murina*) than among all other species (Fig. 1;
161 Supplementary Table 4), which is likely due to their younger evolutionary ages and
162 closer taxonomic relationships of their host species (Figs. 2a and 2c). These
163 rearrangements could have caused incompatibilities between these species, thus
164 preventing gene flow, for species that infect the same host.

165 Comparison of pairwise whole genome alignment identities between species
166 indicates a substantial genetic divergence: 14% dissimilarity in aligned regions between
167 *P. jirovecii* and *P. macacae*; 21% between *P. jirovecii* and *P. oryctolagi*; 22% between *P.*
168 *jirovecii* and *P. canis* Ck1; 15% between *P. wakefieldiae* and *P. carinii*; and 12%
169 between *P. wakefieldiae* and *P. murina* (Supplementary Table 5).

170

171

172

## Speciation history of the *Pneumocystis* genus

These new complete genome data enabled us to examine the relationships between different *Pneumocystis* species and to estimate the timing of speciation events that led to the extant species. We inferred a strongly supported phylogeny of *Pneumocystis* species rooted with outgroups from distantly related fungal subphyla. Our phylogenomic analysis of 106 single-copy orthologs inferred from all assemblies including the fragmented Ck2 strongly supports monophyly of *Pneumocystis* species (100% Maximum likelihood bootstrap values; Fig. 2a), Bayesian posterior probabilities (>0.95; Supplementary Figure 1), and highly significant support from the Shimodaira-Hasegawa test (*18*) ($p < 0.001$; see Methods). An identical phylogeny was recovered using mitochondrial genome data from 33 specimens representing 7 *Pneumocystis* (Supplementary Figure 2). However, we identified unexpected placements of *P. wakefieldiae*, *P. oryctolagi* and *P. canis*. First, *P. wakefieldiae* appears as a sister species of *P. murina* instead of *P. carinii* (which also infects rats) (Fig. 2b). This observation is supported by the higher similarity in genome size (Supplementary Table 3), sequence divergence (Supplementary Table 4), genome structure (Fig. 1; Supplementary Table 5) and higher frequencies of supporting genes (0.64 in 1718 nuclear gene trees examined; Methods) between *P. wakefieldiae* and *P. murina* than between *P. wakefieldiae* and *P. carinii*. These relationships contradict the previous phylogenetic placement of *P. wakefieldiae* as an outgroup of the *P. carinii*/*P. murina* clade (*9*) or a sister species of *P. carinii* (*19*) based on analysis of mitochondrial large and small subunit rRNA genes (mtLSU and mtSSU). The new phylogeny also opposes the prevailing hypothesis for dynamics of host specificity and coevolution within the *Pneumocystis* genus, that is, *P. wakefieldiae* shares with *P. carinii* the same host

196 species (*Rattus norvegicus*) and thus is expected to be more related to *P. carinii* than to *P.*
197 *murina*.

198 Similarly, *P. oryctolagi* would be expected to be phylogenetically closer to rodent
199 *Pneumocystis* than to primate *Pneumocystis*, consistent with the closer phylogenetic
200 relationships of rabbits and rodents to each other than to primates (*20*) (Figs. 2a and 2b).
201 In contrast, *P. oryctolagi* and *P. canis* are more closely related to primate *Pneumocystis*
202 (*P. jirovecii* and *P. macacae*) than rodent *Pneumocystis* (Fig. 2a; Supplementary Figures
203 1 and 2; 100% of tree level support in 1,718 nuclear genes). The phylogenetic
204 discrepancy between *P. oryctolagi* and its host (rabbit) suggests that host switching may
205 have occurred in their distant history.

206 From whole-genome Bayesian phylogenetic estimates (see Methods), the
207 common ancestor of all extant species of the genus emerged around 140 mya (confidence
208 intervals: 180–101 mya; Fig. 2c; Supplementary Figure 1), with a separation of
209 *Pneumocystis* and *Schizosaccharomyces* genera around 512 mya (CI: 822-203 mya)
210 which is consistent with independent estimates of the origin of Taphrinomycota crown
211 group at 530 mya (*21*). The *Pneumocystis* genus thereafter divided into two main clades,
212 P1 consisting of *P. jirovecii*, *P. macacae*, *P. oryctolagi* and *P. canis*, and P2 consisting of
213 species infecting rodents (*P. carinii*, *P. wakefieldiae* and *P. murina*) (Fig. 2b).
214 Subsequent to the divergence of P1/P2, the clade P1 diversified through a series of
215 speciation events leading either to new primate or carnivore species whereas P2 remained
216 localized in rodents. We also found that the divergence time of *Pneumocystis* in the clade
217 P1 predates that of their hosts, that is, the crown of rodent-rabbit-primate *Pneumocystis* is
218 clearly more ancient than the corresponding superorder of mammals (Euarchontoglires)

(Fig. 2c). The pattern in clade P2 is different as the divergence time estimates overlap with those of their hosts (Fig. 2c). On the basis of coalescent estimates, *P. jirovecii* began to split from *P. macacae* at ~62 mya (CI: 69-55 mya) which extended through the Cretaceous-Paleogene mass extinction event at 66 mya, but substantially predates the crown Catarrhini (human-macaque ancestor) of ~20 mya (CI: 24-17 mya; Fig. 2c; Supplementary Figure 1).

**High levels of population differentiation identified from *Pneumocystis* genomes support reproductive isolation**

To understand the genomic divergence landscape of *Pneumocystis* populations, we performed genome-wide differentiation tests ($F_{ST}$, relative population divergence) and nucleotide diversity ($\pi$) (Methods). These analyses used 32 genomic datasets, including 26 publicly available datasets in GenBank for *P. jirovecii*, *P. carinii* and *P. murina* and 6 datasets generated in this study for other four *Pneumocystis* species (Supplementary Note 1; Supplementary Table 2). Of note *Pneumocystis* organisms from macaque, rat and rabbit samples are from infected laboratory or domesticated animals (Supplementary Table 5), and thus do not represent true random representation of natural (e.g. wild) populations. We used a trained version LAST (*22*) to account for interspecies divergence during read mapping and ANGSD (*23*) to derive genotype likelihoods instead of genotypes. Since ANGSD's $F_{ST}$ requires outgroups, we analyzed interspecies divergence between *P. jirovecii*, *P. macacae* and *P. oryctolagi* populations using a sliding window approach of 5-kb and *P. carinii* as an outgroup species (*n* samples = 59). *P. murina* genomic divergence relative to *P. carinii* and *P. wakefieldiae* populations was estimated

242 similarly using *P. jirovecii* as an outgroup species ($n$ = 47). We found high levels of
243 population differentiation among *Pneumocystis* specimens; 71.9% of the *P. jirovecii*
244 genome had a Fixation index ($F_{ST}$) > 0.8 compared to the closest species, *P. macacae*,
245 while 90.2% of the genome had a $F_{ST}$ > 0.8 compared to the extant species *P. oryctolagi*
246 (Supplementary Figure 3). Similarly, 86.3% and 93.7% of the *P. murina* genome had a
247 $F_{ST}$ > 0.8 compared to *P. carinii* and *P. wakefieldiae*, respectively (Supplementary Note
248 1).
249
250 **Analyzing historical hybridization in *Pneumocystis* genus**
251 Topology-based maximum likelihood analysis of 1,718 gene trees using PhyloNet (*33*)
252 found no evidence of statistically significant signals for gene flow among species of clade
253 P1 (*P. jirovecii*, *P. macacae*, *P. oryctolagi* and *P. canis*) (see Methods; Supplementary
254 Figure 4), which indicates that these lineages were reproductively isolated throughout
255 their evolutionary history, consistent with their isoenzyme diversity (*34*). In contrast, we
256 found strong evidence of ancient hybridization in clade P2, possibly between *P. carinii*
257 and *P. wakefieldiae* (Methods; Supplementary Figure 4), which may then have
258 contributed to the formation of the *P. murina* lineage. We hypothesize that *P. murina*
259 might have originated as a hybrid between ancestors of *P. carinii* and *P. wakefieldiae* in
260 rats, and subsequently shifted to mice, possibly owing to the geographic proximity of
261 ancestral rodent populations (for example in Southern Asia (*35*)), which is consistent
262 with the fact that ecological fitting is a major determinant of host switch (*36*). The
263 presumed physiological, cellular and/or immunological similarities among closely related
264 rodent species might also have helped the same *Pneumocystis* species colonizing multiple

closely-related rodent hosts (*10*, *36*). The putative host shift might have been required because of negative selection against *P. murina* specifically in rats, possibly stemming from competition of low-fitness hybrids with parental species as is frequently observed in fungal pathogens (*37*). It is also interesting to note that earlier studies have suggested competition between *P. carinii* and *P. wakefieldiae* in rat colonies (*38*), and further, that *P. wakefieldiae* can no longer be detected in commercial vendors (Cushion et al. unpublished observation), while *P. carinii* can consistently be identified in laboratory rats. However, both *P. carinii* and *P. wakefieldiae* can be found, alone or together, in different species of *Rattus* in Southeast Asia (*10*).

**Gene families and metabolic pathways linked to host specificity**

Gene annotations of *P. macacae* and *P. wakefieldiae* genomes was performed using RNA-Seq paired-end reads to guide *ab initio* gene predictions (Methods). *P. oryctolagi* and *P. canis* genomes were annotated using *ab initio* and homology-based predictions. The predicted protein-coding gene numbers are similar across *Pneumocystis* genomes and range from 3,211 in *P. wakefieldiae* to 3,476 in *P. canis* strain Ck1 (Supplementary Table 3). Nearly all predicted protein coding genes in *P. macacae* (96% of 3,471) and *P. wakefieldiae* (99% of 3,221) genomes have RNA-Seq support. Gene models present a complex architecture with 5.7 to 6.3 exons per gene. High representation of core eukaryotic genes in *P. macacae*, *P. oryctolagi*, *P. canis* and *P. wakefieldiae* provides evidence that these genomes are nearly complete and comparable in completeness to *P. jirovecii*, *P. murina* and *P. carinii* genomes: 86.2 to 93.4% of conserved genes are detectable in all annotated genome assemblies (Supplementary Table 3).

Examination of orthologous genes reveals that ~3,100 orthologous clusters had representative genes from all nine analyzed genome assemblies from seven *Pneumocystis* species (Supplementary Table 3). We found a small number of unique genes in each *Pneumocystis* species ranging from 25 in *P. wakefieldiae* to 204 in *P. oryctolagi* (Supplementary Table 3). Unique genes in most species encode for phylogenetically unrelated proteins with unknown function. A striking exception is observed in *P. macacae* in which nearly all unique proteins are part of a novel undescribed large protein family ($n$ = 190). The members of this new family are enriched in arginine and glycine amino acid residues (denoted RG proteins) (Supplementary Figure 5a) and have no similarities with transposable elements. While RG motifs are often found in eukaryotic RNA-binding proteins (*24*), *P. macacae* RGs do not possess an RNA-binding domain (Pfam domains PF00076, PF08675, PF05670, PF00035), suggesting a different role. In addition, *P. macacae* RGs lack functional annotation except for two proteins that encode a Dolichol-phosphate mannosyltransferase domain (PF08285) and a leucine zipper domain (PF10259), respectively. Of the 190 RGs, 134 have RNA-Seq based gene expression support, including five among the top highly expressed genes (Supplementary Figure 5b). Nearly half of RGs are located at subtelomeric regions and often found in close proximity to *msg* genes (Supplementary Table 6). RG proteins can be grouped in three main clusters (based on OrthoFinder clustering; Methods), have a reticulate phylogeny (Supplementary Figure 5c) and a mosaic gene structure (Supplementary Figure 5d) which suggest frequent gene conversion events. These results suggest that RG proteins may play important roles in *P. macacae* specific biology. Further experiments are ongoing to elucidate the functions of these proteins in *P. macacae*.

To investigate the gene loss patterns in newly sequenced genomes, we compared *Pneumocystis* gene catalogs to those of related Taphrinomycotina fungi. We found that all sequenced *Pneumocystis* species have lost ~40% of gene families present in other Taphrinomycotina (Supplementary Figure 6), and that the metabolic pathways are also very similar among *Pneumocystis* species with a few minor (possibly stochastic) differences (Supplementary Note 2). This strongly suggests that *Pneumocystis* ancestry experienced massive gene losses that occurred before the genus diversification.

To investigate changes in gene content that might explain interspecies differences among the seven *Pneumocystis* species, we searched for expansions or contractions in functionally classified gene sets. We identified Pfam domains with significantly uneven distribution among genomes (Wilcoxon signed-rank test $p < 0.05$). Domains associated with Msg proteins are enriched in *P. jirovecii* and, to a lesser extent in *P. macacae* compared to other species (Fig. 3a). Domains associated with peptidases (M16) are enriched in *P. carinii*, *P. murina* and *P. wakefieldiae*. S8 peptidase family (kexin) is expanded in *P. carinii* as described previously *(13)* with 13 copies whereas all other species have one or three copies (Fig. 3a; Supplementary Figure 7). Although kexin is localized in other fungi to the Golgi apparatus, and in *Pneumocystis* is believed to be involved in the processing of Msg proteins, the expanded copies are predicted to be GPI-anchored proteins, appear to localize to the cell surface; their function is unknown (*25*). *P. carinii* and *P. wakefieldiae* have 13 and 3 copies whereas all other *Pneumocystis* species have only one (Supplementary Figure 7). We found that *P. carinii* kexin genes evolved under strong positive selection ($p = 0.008$) whereas *P. wakefieldiae* kexin genes did not ($p = 0.159$).

Proteins with CFEM (common in fungal extracellular membrane) domains are important for the acquisition of vital compounds in fungal pathogens (*26*). *Pneumocystis* have an unusual high presence of CFEM domains compared to other Taphrinomycotina; each species possesses five proteins containing 2 to 6 domains per protein (Supplementary Figures 8a-c), with no significant differences among different species (*p*-value = 0.057; PF05730.10). Phylogenetic analysis of CFEM domains indicates that *Pneumocystis* species have experienced significantly higher intragenic duplications rates relative to other fungi (Supplementary Figure 8b). These results suggest that multiple CFEM domains were likely already present in the last common ancestor of *Pneumocystis* and were vertically transmitted.

To investigate changes in enzyme gene content that might account for inter-species differences among *Pneumocystis* species, we searched for enzymes that show clear differences among species, which are represented by Enzyme Commission numbers (ECs) (Fig. 3b). We found 34 ECs, which include 14 that are highly conserved in *P. jirovecii* but have a patchy distribution in other members of clade P1 (*P. macacae*, *P. canis* and *P. oryctolagi*) and are lost in clade P2 (*P. carinii*, *P. murina* and *P. wakefieldiae*). Most of these 14 ECs are assigned to the biosynthesis of antibiotics or secondary metabolites and vitamin B6 metabolism according to KEGG pathways. The latter pathway seems only functional in P2 clade (Supplementary Note 2).

**Intron evolution**

We analyzed 1,211 one-to-one gene orthologs shared by all sequenced *Pneumocystis* and other Taphrinomycotina fungi (Supplementary Figure 9a). A total of 9,080 homologous sites within 1,211 alignments were identified (Supplementary Figure 9b). While intron densities are similar among *Pneumocystis* species (ranging from 4,842 in *P. macacae* to 5,289 in *P. murina*), they are markedly more elevated compared to related Taphrinomycotina, including *Neolecta irregularis* (*n* = 4,202 introns), *Schizosaccharomyces pombe* (*n* = 862) and *Taphrina deformans* (*n* = 639) (Supplementary Fig. 11b). Predictions of ancestral intron densities show that the *Pneumocystis* common ancestor had at least 5,341 introns, of which 37% were novel i.e. not found in other Taphrinomycotina (Supplementary Figure 9c). This is in contrast to other fungi; ~26% of *Neolecta* introns were independently acquired whereas *S. pombe* and *T. deformans* genomes have experienced significant intron losses, which is consistent with previous studies (*31, 32*). These results suggest the emergence of *Pneumocystis* genus was preceded by a significant amount of intron gain.

**Positive selection footprints in *P. jirovecii* genes**

We tested the hypothesis that *P. jirovecii* has adapted specifically to humans after its separation with *P. macacae*, and that there will be footprints of directional selection in the genome that point to the molecular mechanisms of this adaptation. To infer *P. jirovecii*-specific adaptive changes, we compared the *P. jirovecii* one-to-one orthologs to those of *P. macacae* and *P. oryctolagi* using the branch-site likelihood ratio test (*39*). Positive selection was identified as an accelerated non-synonymous substitution rate. The

test identified 244 genes (out of 2,466) with a signature of positive selection in the human pathogen *P. jirovecii* alone (Bonferroni corrected *p*-value < 0.05; Supplementary Table 7). Gene Ontology enrichment analysis of these genes with accelerate rates identified significant enrichment for the biological process "cellular response to stress" (adjusted using Benjamini-Hochberg *p*-value =1.9 x $10^{-6}$) and the molecular function "potassium channel regulator activity" ($p$ = 2.8 x $10^{-10}$). Among the 244 genes, 197 are conserved in all *Pneumocystis* genomes available whereas 47 are absent in clade P2 only (*P. carinii*, *P. murina* and *P. wakefieldiae;* Fig. 2b). While the latter set of genes encode proteins of unknown function, analysis of Pfam domains shows a significant enrichment in the biological process "nucleoside phosphate biosynthetic" process ($p$ = 9.9 x $10^{-5}$) and the molecular function "carbon-nitrogen lyase activity" ($p$ = 2.8 x $10^{-10}$). Further investigations will be required to determine the precise functions of these genes.

**Subtelomeric gene families**

Until recently, the only in-depth data on the subtelomeric gene families in *Pneumocystis* have come from the *P. jirovecii*, *P. carinii* and *P. murina* (*13*, *40*). These genes, including *msg* and kexin, are believed to be important for antigenic variation, and are well represented in the assemblies of *P. macacae, P. oryctolagi, P. canis* and *P. wakefieldiae*. We provide a comprehensive analysis of their composition and evolution that complements our recent publication (*41*).

*P. macacae* subtelomeres encode numerous arrays of Msg and RG proteins (Supplementary Table 7). Phylogenetic analysis of adjacent genes revealed only a few instances of recent paralogs, which suggests that most of the duplications and subsequent

positional gene arrangements are ancient. Three *P. macacae* subtelomeric regions have a nearly perfect synteny in *P. jirovecii* with the only difference being the absence of RG proteins in *P. jirovecii* (Supplementary Table 7). *P. oryctolagi* subtelomeres tend to be enriched in orphan genes that are not members of the Msg superfamily, and are of unknown function. *P. canis* subtelomeres are enriched in Msg-C family (see Msg section below). *P. wakefieldiae* subtelomeres are enriched in *msg* genes, though their types are distinct from those of *P. carinii* and *P. murina*.

**Evolution of *msg* genes**

Up to 6% of the *Pneumocystis* genomes are comprised of copies of the *msg* superfamily, which are believed to be crucial mediators of pathogenesis through antigenic variation and interaction with the host cells. The superfamily is classified into five families A, B, C, D and E based on protein domain architecture, phylogeny and expression mode (*13, 40, 41*). The A family is the largest of the five, has been subdivided into three subfamilies (A1, A2 and A3) and is generally thought to contribute to antigenic variation. Their protein products contain cysteine-rich domain classified as N1 and M1 to M5.

To investigate the origin of *msg* genes, we used previously developed Hidden Markov Models (*13*) to search for corresponding gene models in the assemblies of *P. macacae*, *P. oryctolagi*, *P. canis* and *P. wakefieldiae* and combined these data with previously published *msg* sequences annotated in *P. jirovecii*, *P. carinii* and *P. murina* genomes (*13, 41*). Of note, in this study only a subset of *msg* genes were assembled for *P. oryctolagi*, *P. canis* and *P. wakefieldiae* due to difficulties in assembling highly similar short reads from Illumina sequencing exclusively while a potentially complete set of *msg* genes were assembled for *P. macacae* using Illumina and Nanopore reads

(Supplementary Table 3). The number of full-length *msg* genes available ranges from 9 in *P. oryctolagi* to 161 in *P. jirovecii*. Sequence-based clustering and phylogenetic analyses of all *msg* genes ($n$ = 482) revealed that: (i) there is no evidence of inter-species transfer among *Pneumocystis* species (Figs. 4b to d; Supplementary Figure 10), (ii) *msg* genes may have a polyphyletic origin, i.e. distinct families were present in most recent ancestors of *Pneumocystis* (Supplementary Figure 10a); (iii) *msg* genes experienced significant amount of recombination early in their history as estimated by phylogenetic network analysis (Supplementary Figures 10b and c).

The evolution of *msg* genes between clades P1 and P2 is not uniform among *Pneumocystis* species and instead has clear differences between them. While some gene expansions are relatively recent (for example, *msg* families A, C and D) other expansions (*msg* families E and B) occurred before the emergence of *Pneumocystis* genus itself (Supplementary Figure 11). Subsets of *msg* genes show strong host specific sequence diversification (Fig. 4a), such as the current A family have emerged relatively recently 43 mya ago (CI: 58-28 mya) compared to the emergence of the genus at 140 mya ago (see Methods; Supplementary Figure 11). The A1 subfamily displays a substantial expansion in all species (Fig. 4a) and is subject to significant intra-species recombination (Figs. 4b to d), which suggest that *Pneumocystis* most recent ancestor may have develop a pre Msg-A family, which then evolved through duplication and recombination after the separation of species.

The A3 subfamily has expanded only in clade P1 (especially in *P. jirovecii*) whereas A2 has expanded only in clade P2 (*P. carinii*, *P. murina* and to a lesser extent in *P. wakefieldiae*) (Fig. 4a). Although all members of the A family might have a shared

450 deep ancestry, we found no evidence suggesting that the A1, A2, A3 subfamilies are
451 directly derived from one another (Supplementary Figure 10).

452 The *msg* B family underwent a net independent expansion in *P. macacae* (*n* = 10)
453 and *P. jirovecii* (*n* = 12), while being reduced to only one copy in *P. oryctolagi* and *P.*
454 *canis*, and being completely absent in *P. wakefieldiae*, *P. carinii* and *P. murina* (Fig. 4a).
455 Using Bayesian estimates, we estimated the origin of B family to be older than the
456 *Pneumocystis* genus itself (~211 versus 140 mya; Supplementary Figure 11). While a half
457 of the B family members are located in subtelomeric regions in *P. jirovecii* and *P.*
458 *macacae*, we found no evidence of recent inparalogs, which is consistent with their
459 ancient origin. B family members lack predicted GPI anchor or transmembrane domain
460 and have a shorter proline-rich motif compared to other *msg* families. Many of the *msg* B
461 family members have a predicted secretory signal (13/25), with more in *P. jirovecii* than
462 in *P. macacae* (7 vs. 3 copies). These data suggest that at least some members of the B
463 family may be secreted effectors.

464 The *msg* D family is expanded only in *P. macacae* and *P. jirovecii*. The D family
465 emerged at ~69 mya (CI: 109-40 mya) before the split of these two species
466 (Supplementary Figure 11), thus suggesting a role in adaptation to primates similar to the
467 A3 subfamily. In contrast, the E family, which is conserved in all species, is much more
468 ancient at ~311 mya ago (CI: 541-158 mya), again preceding the emergence of the genus
469 (Supplementary Figure 11).

470 *P. jirovecii* and *P. macacae* have a significantly larger number of *msg*-associated
471 cysteine-rich domains than other *Pneumocystis* species (Fig. 5a) and also a much greater
472 sequence diversity per domain than other *Pneumocystis* species (Fig. 5c). Domain

473 sequences cluster independently, with each cluster containing sequences from all
474 *Pneumocystis* species (Fig. 5b). Domains M1 and M3 are more closely related to each
475 other than other domains, which suggests a relatively recent duplication. These results
476 suggest that the all domains are likely to appear in the *Pneumocystis* ancestor and
477 underwent a series of lineage specific expansions. The paucity of domains in *P.*
478 *oryctolagi*, *P. canis* and *P. wakefieldiae* might reflect an interaction with host cells
479 different than other species. Alternatively, these differences could represent incomplete
480 sets of Msgs in the former species.
481
482 **Conclusions**
483 In the current study, we have produced high-quality genome assemblies and used them to
484 investigate the speciation and host specific adaptation of multiple members of the
485 *Pneumocystis* genus. We have established a robust phylogeny, presented genomic
486 differences among species, identified a possible introgression among rodent-hosted
487 *Pneumocystis* species, and discovered two phylogenetically distinct *Pneumocystis*
488 lineages in dogs. Our analysis suggests that successful infection of humans by *P. jirovecii*
489 has a deep evolutionary root accompanied by important genomic modifications.
490 Surprisingly, analysis of core genomic regions of nuclear genomes did not identify clear
491 differences that are suggestive of mechanisms for host-specific adaptation; instead it is
492 the highly polymorphic multicopy gene families in subtelomeric regions that appear to
493 account for this adaptation.
494 Based on our analysis, we propose the following series of events for the
495 emergence and adaptation of *P. jirovecii* as a major human opportunistic pathogen (Fig.

6). First, there was a major shift of a pre-*Pneumocystis* lineage (possibly a soil- or plant-adapted organism) to mammals, which led to a significant genome reduction but with a significant proliferation of introns and expansions of cysteine-rich domain-containing proteins involved in immune escape and nutrient scavenging from hosts. *Pneumocystis* genomes encode multiple gene families that have experienced a rapid accumulation of mutations favoring fungal replication in mammals. Each *Pneumocystis* species has employed different strategies to adapt to their host including lineage-specific expansions of shared gene families such as *msg* A1, A3 and D in *P. jirovecii* or gain and expansion of RG proteins in *P. macacae*. In addition, some shared gene families also have acquired different properties (e.g., transmembrane domain and secreted signals) potentially contributing to host specificity. Our data point to the possibility that chromosomal rearrangements may play a role in the inhibition of gene flow between *P. jirovecii* and *P. macacae* leading to their speciation. The absence of a reliable culture method and the inability to genetically manipulate *Pneumocystis* prevents directly testing our model. Moreover, for the genes that we have now implicated in the process of host adaptation, only a few have been functionally characterized. Future studies on the role of these genes will be important to elucidate the molecular basis of in host specific adaptation by *Pneumocystis* pathogens.

By untangling the co-evolution of *Pneumocystis* species with their mammalian hosts, we show that this evolution is more complex than portrayed by a strict co-evolutionary framework. The potential relaxation of strict host specificity in small mammals colonized by *Pneumocystis* could be explained as well by the fact that, in the coevolution theory, parasites infecting rodents (small-bodied with short lifespans, high

519 reproduction rates, and high population densities) have lower host specificity than those
520 adapted to long-lived large mammals with more stable population densities (*42*). Our
521 analyses documented rare instances of pathogen speciation while sharing the same host
522 (rats and dogs), which is equivalent to a speciation in sympatry (without geographical
523 isolation). This work predicts novel and critical aspects of the genetic basis of host
524 adaptation by *P. jirovecii*, the only fungal pathogen known to have adapted to living
525 exclusively in human lungs. Future studies further expanding the sampled *Pneumocystis*
526 genomes across the diversity of mammals, will be key to further understanding molecular
527 basis of host specificity. The evolutionary processes that gave rise to the obligate
528 biotrophic lifestyles of *Pneumocystis* within its host remain important future research
529 questions (*43, 44*). The next important steps will also include the study of the influence of
530 host biology on *Pneumocystis* adaptation, the genetic mechanisms underlying pathogen
531 host shifts, and the genetic incompatibility between coexisting pathogens (e.g. *P. carinii*
532 and *P. wakefieldiae* in rats).
533

534 **Material and Methods**

535 **Experimental Design and *Pneumocystis* sample sources**

536 Animal and human subject experimentation guidelines of the National Institutes of
537 Health (NIH) were followed in the conduct of this study. Studies of human and
538 mouse *Pneumocystis* infection were approved by NIH Institutional Review Board (IRB)
539 protocols 99-I-0084 and CCM 19-05, respectively. The collection and processing of a
540 single *P. jirovecii* human bronchoalveolar lavage sample from China (Pj55) was
541 approved by the IRB of the First Affiliated Hospital of Chongqing Medical University,

542 China (protocol no. 20172901). Written informed consent was obtained from the patient
543 for the participation in this study. The authors confirmed that personal identity
544 information of the patient data was unidentifiable from this report. The National Institute
545 of Allergy and Infectious Diseases (NIAID) Division of Intramural Research Animal
546 Care and Use Program, as part of the NIH Intramural Research Program, approved all
547 experimental procedures pertaining to the macaques (protocol LVD 26). Nonhuman
548 primate study protocols were approved by the Institutional Animal Care and Use
549 Committee of the University of California, Davis (protocol no. 7092), the Tulane
550 National Primate Research Center (TNPRC) and the Institutional Animal Care and Use
551 Committee (IACUC) (protocol no. P0351R). Studies of
552 rabbit *Pneumocystis* infection were reviewed and approved by the Institutional Animal
553 Care and Use Committee of the University of Michigan (protocol no. RO00008218). For
554 rabbit samples obtained France, the conditions for care of laboratory animals stipulated in
555 European guidelines were followed (See: Council directives on the protection of animals
556 for experimental and other scientific purposes, and J. Off. Communautés Européennes,
557 86/609/EEC, 18 December 1986, L358). Samples from *Pneumocystis* infected dog were
558 collected as diagnostic samples and approved for only for research purpose. The owner's
559 consents for using samples and data were obtained on admission of the case and no
560 further ethics permission was required because it was a routine diagnostic case and did
561 not qualify as an animal experiment. Studies of rat *Pneumocystis* infection were approved
562 by the Veteran Affairs animal protocol (VA ACORP #17-12-05-01). Clinical information
563 and demographic data of the groups of individuals are presented in Supplementary Table
564 1.

565 Three *P. jirovecii* samples were obtained as bronchoalveolar lavage from patients
566 at the NIH Clinical Center in Bethesda, MD, USA and Chongqing Medical University in
567 Chongqing, China.

568 Six *P. macacae* samples were obtained as frozen lung tissues or formalin fixed
569 paraffin embedded (FFPE) tissue sections prepared from SIV-infected rhesus macaques
570 at the NIH Animal Center, Bethesda, Maryland ($n$ = 2), the Tulane National Primate
571 Research Center, Covington, Louisiana ($n$ = 3), and the UC Davis California National
572 Primate Research Center, Davis, California, USA ($n$ = 1).

573 Four *P. oryctolagi* samples were obtained as frozen lung tissues from one rabbit
574 with severe combined immunodeficiency at the University of Michigan, Ann Arbor,
575 Michigan, USA, or as DNA from two corticosteroid treated rabbits and one rabbit with
576 spontaneous *Pneumocystis* infection at the Institut Pasteur de Lille and the Institut
577 National de la Recherche Agronomique de Tours Pathologie Aviaire et Parasitologie,
578 Tours, France.

579 *P. canis* samples were obtained as DNA from one Cavalier King Charles Spaniel
580 dog at the University of Helsinki, Finland and one Whippet mixed-breed at the University
581 of Veterinary Medicine, Vienna, Austria.

582 *P. murina* organisms were obtained from heavily-infected CD40L-KO mice
583 following a short-term *in vitro* culture. Genomic data obtained from *P. murina* isolates
584 were combined with previously sequenced public data (Supplementary Table 2) and used
585 for population genomics analysis (section "Speciation history of the *Pneumocystis* genus"
586 and Supplementary Note 1).

One frozen cell pellet and 4 agarose gel blocks containing *P. wakefieldiae* and *P. carinii* were obtained from immunosuppressed rats (one gel block per rat) housed at the Cincinnati VA Medical Center, Veterinary Medicine Unit, Cincinnati, Ohio.

**Genome sequencing, assembly and annotation**

Genomic DNA in agarose gel blocks was extracted using the Zymoclean Gel DNA Recovery Kit (Zymo Research). Genomic DNA in FFPE sections was extracted using the AllPrep DNA/RNA FFPE Kit (Qiagen). Genomic DNA in frozen lung tissues from two *P. macacae*-infected macaques and one *P. oryctolagi*-infected rabbit was extracted using the *Pneumocystis* DNA enrichment protocol as described elsewhere (*5, 13*). Genomic DNA in bronchoalveolar lavage samples from *P. jirovecii*-infected patients was extracted using the MasterPure Yeast DNA purification kit (Epicentre Biotechnologies, Madison, WI, USA). Total RNAs for *P. macacae*, *P. wakefieldiae* and *P. murina* were isolated using RNeasy Mini kit (Qiagen).

For DNA samples with small quantity, including three *P. oryctolagi* samples (RABF, RAB1 and RAB2B) and one *P. jirovecii* sample (RU817), we performed whole genome amplification prior to Illumina sequencing. Five microliters of each DNA sample were amplified in a 50-ul reaction using an Illustra GenomiPhi DNA V3 DNA amplification kit (GE Healthcare, United Kingdom).

Genomic DNA samples were quantified using Qubit dsDNA HS assay kit (Invitrogen) and NanoDrop (ThermoFisher). RNA samples integrity and quality were assessed using Bioanalyzer RNA 6000 picoassay (Agilent). The identities of *Pneumocystis* organisms were verified by PCR and Sanger sequencing of mtLSU before

high throughput sequencing. For most of the DNA samples, at least one microgram of each DNA or RNA (depleted of ribosomal RNA using Illumina Ribo-Zero rRNA Removal Kit) sample was sequenced commercially using the Illumina HiSeq2500 platform with 150 or 250-base paired-end libraries (Novogene Inc, USA) or for one DNA sample of *P. jirovecii* from a Chinese patient using a single-read SE50 library using the MGISeq 2000 platform (MGI Tec, China). Raw reads statistics and NCBI SRA accession numbers are presented in Supplementary Material (Data access section) and Supplementary Table 2.

Adapters and low-quality reads were discarded using trimmomatic v0.36 (*45*) with the parameters "-phred33 LEADING:3 TRAILING:3 SLIDINGWINDOW:4:15 MINLEN:36". Host DNA and other contaminating sequences were removed by mapping against host genomes using Bowtie2 v2.4.1 (*46*). Filtered Illumina reads were assembled *de novo* using Spades v3.11.1 (*47*). Details for host DNA sequences removal, *Pneumocystis* reads recovery and *de novo* assembly protocols are presented in Supplementary Material. Completeness of assemblies was estimated using BUSCO v9 (*48*), FGMP v1.0.1 (*49*) and CEGMA v2.5 (*50*).

Nanopore sequencing was performed on *P. macacae* DNA samples prepared from a single heavily infected macaque (P2C) with ~68% *Pneumocystis* DNA based on prior Illumina sequencing (Supplementary Table 2). High molecular weight genomic DNA fragments were isolated using the BluePippin (Sage Science) with the high-pass filtering protocol. A DNA library was prepared using the rapid Sequencing kit (SQK-RAD0004) from Oxford Nanopore Technologies (Oxford, UK) and loaded in the MinION sequencing device. Host reads were removed by mapping to the Rhesus macaque genome

(NCBI accession number GCF_000772875.2_Mmul_8.0.1) using Minimap2 v2.10 (*51*). Unmapped reads were aligned to the draft version of *P. macacae* assembly built previously using Illumina data (Supplementary Methods) with ngmlr v0.2.7 (*52*). A total of 1,633,376 nanopore reads were obtained, of which ~5% were attributed to *Pneumocystis* (27-fold coverage), which is much less than the 68% based on Illumina data (Supplementary Table 2). This suggests that many *P. macacae* genomic DNA fragments were too short to pass the size selection filter. *Pneumocystis* nanopore reads were assembled using Canu v.1.8.0 (*53*), overlapped with the assembly using Racon v.1.3.3 (*54*) and polished with Pilon v1.22 (*55*) using the Illumina reads aligned with BWA MEM v0.7.17 (*56*).

Illumina RNA-Seq of the *P. macacae* sample P2C yielded 22 millions reads, of which ~92% were attributed to *Pneumocystis* (Supplementary Table 2). Filtered reads were mapped to the *P. macacae* assembly using hisat2 v2.2.0 (*57*), sorted with SAMtools v1.10 (*58*) and filtered with PICARD v2.1.1 (http://broadinstitute.github.io/picard). *De novo* transcriptome assembly of filtered reads was performed with Trinity (*59*). Quantification of transcript abundance was performed using Kallisto v0.46.1 (*60*). *P. wakefieldiae* (2A) and *P. murina* RNA-Seq data were processed similarly (Supplementary Table 2).

DNA transposons, retrotransposons and low complexity repeats were identified using RepeatMasker (*61*), RepBase (*62*) and TransposonPSI (http://transposonpsi.sourceforge.net). *Pneumocystis* telomere motif “TTAGGG” (*16*) was searched using “FindTelomere” (available at https://github.com/JanaSperschneider/FindTelomeres). The genomes of *P. carinii* strain

Ccin (*14*) and strain SE6 (*12*) were scaffolded with Satsuma (*63*) using the *P. carinii* strain B80 as reference genome (*13*). *P. macacae*, *P. oryctolagi*, *P. canis* Ck1, *P. canis* A, *P. wakefieldiae*, and *P. carinii* (strains Ccin and SE6) genome assemblies were annotated using Funannotate v1.5.3 (DOI 10.5281/zenodo.1134477). The homology evidence consists of fungal proteins from UniProt (*64*) and BUSCO v9 fungal proteins (*48*). For *P. macacae* and *P. wakefieldiae*, RNA-Seq mapping files (BAM) and *de novo* transcriptome assemblies were used as hints for AUGUSTUS (*65*). *Ab initio* predictions were performed using GeneMark-ES (*66*). All evidences were merged using EvidenceModeler (*67*). *Taphrina* genomes (*T. deformans*, *T. wiesneri*, *T. flavoruba* and *T. populina* (*32*, *68*)) and *P. canis* Ck2 were annotated using MAKER2 (*69*) because predicted gene models showed a better quality than those obtained from Funannotate. MAKER2 integrates *ab initio* prediction from SNAP (*70*), AUGUSTUS built-in *Pneumocystis* gene models (*71*) and GeneMark-ES as well as BLAST- based homology evidences from a custom fungal proteins database. GPI prediction was performed using PredGPI (*72*), big-PI (*73*) and KohGPI (*74*). Signal peptide leader sequences and transmembrane helices were predicted using Signal-P version 5 (*75*) and TMpred (*76*), respectively. Protein domains were inferred using Pfam database version 3.1 (*77*) with PfamScan (https://bio.tools/pfamscan_api). Domain enrichment analysis was performed using dcGOR version 1.0.6 (*78*). PRIAM (*79*) release JAN2018 was used to predict ECs using the following options: minimum probability > 0.5, profile coverage > 70%, check catalytic – TRUE and e-value < $10^{-3}$. *Pneumocystis* mitochondrial genome assembly and annotations are described in Supplementary Material. Three dimensional (3D) protein

678 structure prediction of Msg proteins was performed using DESTINI (*80*) and visualized
679 with PyMol (www.pymol.org).
680
681 **Comparative genomics**
682 All genomes were pairwise aligned to the *Pneumocystis jirovecii* strain RU7 genome
683 NCBI accession GCF_001477535.1 (*13*) using LAST version 921 (*22*) with the MAM4
684 seeding scheme (*81*). One-to-one pairwise alignments were created using maf-swap
685 utility of LAST package and merged into a single multi-species whole genome alignment
686 using LAST's maf-join utility. Pairwise rearrangement distances in terms of minimum
687 number of rearrangements were inferred using GRIMM (*82*) and Mauve (*83*).
688 Breakpoints of genomic rearrangements were refined with Cassis (*84*) and annotated
689 using BEDtools (*85*) 'annotate' command. Average pairwise genome-wide nucleotide
690 divergences were computed with Minimap2 (*51*). Synteny visualization was carried out
691 using Synima (*86*). Msg protein similarity networks were based on global pairwise
692 identity obtained from pairwise alignments of full length proteins using Needle (*87*) or
693 BLASTp (*88*) identity scores for individual protein domains. The networks presented in
694 Figures 4 and 5 were generated using the Fruchterman Reingold algorithm as
695 implemented in Gephi 0.9.2 (*89*).
696 To investigate the evolution of introns in *Pneumocystis* species, we identified
697 unambiguous one-to-one orthologous clusters using reciprocal best Blast hit (e-value of
698 $10^{-10}$ as cut off) in seven *Pneumocystis* species as well as in three other Taphrinomycotina
699 fungi : *S. pombe*, *T. deformans* and *N. irregularis*. Intron position coordinates were
700 extracted from annotated genomes using Replicer (*90*) and projected onto protein

multiple alignments using custom scripts. Homologous splice sites in annotated protein sequence alignments were identified using MALIN (*91*). We required at least 11 unambiguous splicing sites and 5 minimal non-gapped positions. A potential splice was considered unambiguous if the site has at least 5 nongaps positions in the aligned sequences in both the left and right sides. MALIN uses a rates-across sites markov model with branch specific gain and loss rates to infer evolution of introns. Gain and loss rates were optimized through numerical optimizations. Fungi have a strong tendency to intron loss with few exceptions (e.g. *Cryptococcus*) whereas gain of intron is relatively rare. Thus, we penalized intron gain and set the variation rate to 4/3 for loss and gain levels. Intron evolutionary history was inferred using a posterior probabilistic estimation with 100 bootstrap support values.

**Phylogenomics**

Orthologous gene families were inferred using OrthoFinder v.2.3.11 (*92*). In addition to *Pneumocystis* and *Taphrina* species, the predicted proteins for the following species were downloaded from NCBI: *Neolecta irregularis* (accession no. GCA_001929475.1), *S. pombe* (GCF_000002945.1), *S. cryophilus* (GCF_000004155.1), *S. octosporus* (GCF_000150505.1), *S. japonicus* (GCF_000149845.2), *Saitoella complicata* (GCF_001661265.1), *Neurospora crassa* (GCF_000182925.2), *Cryptococcus neoformans* (GCF_000149245.1), *Rhizopus oryzae* (GCA_000697725.1) and *Batrachochytrium dendrobatidis* (GCF_000203795.1). Single-copy genes were extracted from OrthoFinder output ($n$ = 106) and concatenated into a protein alignment containing 458,948 distinct alignment patterns (i.e. unique columns in the alignment) with a gap

724 proportion of 12.2%. Maximum likelihood tree analysis was performed using RAxML v
725 8.2.5 (*93*) with 1,000 bootstraps as support values. The LG model (*94*) was selected as
726 the best amino acid model based on the likelihood PROTGAMMAAUTO in RAxML.
727 106 gene trees were estimated from each of the single copy genes. The Shimodaira-
728 Hasegawa test (*18*) was performed on the tree topology for each of the gene trees and the
729 concatenated alignment using IQ-Tree (*95*) with 1,000 RELL bootstrap replicates.
730 To infer the species phylogeny using mitochondrial genomes, protein coding
731 genes were extracted, aligned using Clustal Omega (*96*), and concatenated. The resulting
732 alignment was used to infer phylogeny using IQ-Tree v.1.6 (*97*) with TVM+F+I+G4 as
733 the Best-fit substitution model and 1,000 ultrafast bootstraps and SH-aLRT test. A total
734 of 33 mitogenomes from seven *Pneumocystis* species were used: *P. jirovecii* [*n* = 18
735 including 3 sequences from this study and four from previous studies (*5*, *12*, *17*)], *P.*
736 *macacae* (*n* = 4), four *P. oryctolagi* (*n* = 4), *P. canis* [*n* = 4, (*17*, *98*)], *P. carinii* [*n* = 2,
737 (*17*, *98*)], *P. murina* [ *n* = 1, (*17*)] and *P. wakefieldiae* (*n* = 1).
738 Phylogenetic reconciliations of species tree and gene trees were performed using
739 Notung (*99*). Ancestral reconstruction of gene family's history was performed using
740 Count (*100*). Phylogenetic network for Msg protein families was inferred using SplitTree
741 (*101*). The detection of putative mosaic genes was performed using TOPALi v2.5 (*102*).
742
743 **Phylodating**
744 Single-copy orthogroup nucleotide sequences were aligned using MACS v0.9b1 (*103*).
745 Highly polymorphic *msg* sequences were excluded using BLASTn (*88*) with an e-value
746 of $10^{-5}$ as cutoff against 479 published *msg* sequences (*13*). We inferred the divergence

747 timing using two datasets: (1) 24 single-copy nuclear gene orthologs shared by all
748 *Pneumocystis* and *S. pombe*; and (2) 568 nuclear genes found in all *Pneumocystis* species.
749 BEAST inputs were prepared using BEAUTi v2.5.1 (*104*). Unlinked relaxed lognormal
750 molecular clock models (*105*, *106*) and calibrated birth-death tree priors (*107*) were used
751 to estimate the divergence times and the credibility intervals. The substitution site model
752 HKY was applied (*108*). Three secondary calibration priors were used: (i) *P. jirovecii*/*P.*
753 *macacae* divergence with a median time of 65 mya as 95% highest posterior density
754 (HPD) (*5*)), (ii) the emergence of the *Pneumocystis* genus at a minimum age of 100 mya
755 (*4*), and (iii) the *Schizosaccharomyces – Pneumocystis* split at ~ 467 mya (*109*). For the
756 dataset 2, the 568 gene alignments were concatenated in a super alignment with 568
757 partitions, with each partition defined by one gene. Gene partitions were collapsed using
758 PartitionFinder v2.1.1 (*110*) with the "greedy" search to find optimal partitioning scheme.
759 The alignment was split in three partitions in BEAST. Three independent runs for each
760 dataset were performed separately for 60 million generations using random seeds. Run
761 convergence was assessed with Tracer v1.7.1 (minimum effective sampling size of 200
762 with a burn-in of 10%). Trees were summarized using TreeAnnotator v.2.5.1
763 (http://beast.bio.ed.ac.uk/treeannotator) and visualized using FigTree v.1.4.4
764 (http://tree.bio.ed.ac.uk/software/figtree) to obtain the means and 95% HPD. Host
765 divergences were obtained from the most recent mammal tree of life (*6*), available at
766 http://vertlife.org/data/mammals. The dating of fungal gene families was performed
767 similarly.
768
769 **Population genomics**

Sequence data sources and primary statistics are presented in Supplementary Table 2. Adapter sequences and low-quality headers of base sequences were removed using Trimmomatic (*45*). Interspecies reads alignment was performed using LAST (*22*) with the MAM4 seeding scheme (*81*). Alignments were processed by last-split utility to allow inter species re-arrangements, sorted using SAMtools v1.10 (*58*). Duplicates were removed using and PICARD v2.1.1. To compute the $F_{ST}$ and nucleotide diversity (Watterson, pairwise, FuLi, fayH, L), we calculated the unfolded site frequency spectra for each population using the Analysis of Next Generation Sequencing Data (ANGSD) (*23*). Site frequency spectra was estimated per base site allele frequencies using ANGSD (*23, 111*). Hierarchical clustering was performed using ngsCovar (*112*). All data were formatted to fit a sliding windows of 1-10 kb using BEDTools (*113*). For each window, an average value of the statistics was calculated using custom scripts.

**Gene flow inference**

To infer a phylogenetic network, we used 1,718 one-to-one orthologs from gene catalogs of seven *Pneumocystis* species using reciprocal best BLASTp hit with an e-value of $10^{-10}$ as cut off. Sequences from each orthologous group were aligned using Muscle (*114*). Alignments with evidence of intragenic recombination were filtered out using PhiPack (*115*) with a p-value of 0.05 as cut off. For each aligned group a maximum likelihood (ML) tree was inferred using RAxML-ng (*116*) with GTR+G model and 100 bootstrap replicates, and Bayesian tree was generated using BEAST2 (*104*). ML trees were filtered using the following criteria: 0.9 as the maximum proportion of missing data, 100 as the minimum number of parsimony-informative sites, 50 as the minimum bootstrap node-

793 support value and 0.05 as the minimum p-value for rejecting the null hypothesis of no
794 recombination within the alignment. BEAST trees with an effective sampling size < 200
795 were removed. Filtered trees were summarized using Treannotator
796 (https://www.beast2.org/treeannotator/). Summary trees with an average posterior support
797 inferior to 0.8 were discarded. Species network was inferred using PhyloNet option
798 "InferNetwork_MPL" (*33*) with prior reticulation events ranging from 1 to 4.
799 Phylogenetic networks were visualized using Dendroscope 3 (*117*).
800 The highest probability network inferred a hybridization between *P. carinii* and *P.*
801 *wakefieldiae* leading to *P. murina* followed by a backcrossing between *P. murina* with *P.*
802 *wakefieldiae* (log probability = -12759.4). Analysis of tree topology frequencies revealed
803 that 64% of the trees were consistent with the topology of (*P. carinii*, (*P. murina*, *P.*
804 *wakefieldiae*)), 28% with the topology of (*P. wakefieldiae*, (*P. carinii*, *P. murina*)) and
805 8% with the topology of (*P. murina*, (*P. carinii*, *P. wakefieldiae*)).
806
807 **Detection of positive selection**
808 To search for genes that have been subjected to positive selection in *P. jirovecii* alone
809 after the divergence from *P. macacae*, we used the branch-site test (*39*) as implemented
810 in PAML (*118*) which detects sites that have undergone positive selection in a specific
811 branch of the phylogenetic tree (foreground branch). A set of 2,466 orthologous groups
812 between *P. jirovecii*, *P. macacae* and *P. oryctolagi* was used for the test. $d_N/d_S$ ratio
813 estimates per branch per gene were obtained using Codeml (PAML v4.4c) with a free
814 ratio model of evolution. This process identified 244 genes with a significant signal of
815 positive selection only in *P. jirovecii* ($d_N/d_S > 1$).

816

817 **Statistical analysis, custom scripts and figures**

818 All custom bioinformatic analyses were conducted using Perl v5.26.0

819 (http://www.perl.org/) or Python v.3.6 (http://www.python.org) scripts. Pipelines were

820 written using Snakemake v5.11.2 (*119*). Custom scripts and pipelines are available

821 https://github.com/ocisse/pneumocystis_evolution. Statistical analyses were conducted in

822 R version 3.3.2 (*120*). Phylogenetic trees with geological time scale were visualized

823 using strap version 1.4 (*121*). Sequence motifs were visualized using WebLogo (*122*).

824 Multi-panel figures were assembled in Inkscape (https://inkscape.org). Icon credit in

825 Figure 6: Anthony Caravaggi under the license https://creativecommons.org/licenses/by-

826 nc-sa/3.0/ (mouse), Sam Fraser-Smith (vectorized by T. Michael Keesey) (dog).

827 https://creativecommons.org/licenses/by/3.0/. Anthony Caravaggi

828 https://creativecommons.org/licenses/by-nc-sa/3.0/ (rabbit).

829

830 **Supplementary Materials**

831 Supplementary Methods.

832 Data access.

833 Note S1. Population genomics analysis.

834 Note S2. Metabolic pathways.

835 Fig. S1. The maximum clade credibility tree of *Pneumocystis* species.

836 Fig. S2. Maximum likelihood phylogeny constructed using a concatenated dataset of 15

837 protein coding genes from 33 *Pneumocystis* mitochondrial genomes.

838 Fig. S3. Genome-wide scans for footprints of natural selection in *Pneumocystis*.

839 Fig. S4. Evidence of ancient gene flow in rodent *Pneumocystis* only.

840 Fig. S5. Evolution of arginine-glycine (RG) rich proteins in *P. macacae*.

841 Fig. S6. Heatmap showing gene family distribution in *Pneumocystis*.

842 Fig. S7. Expansion of kexin peptidase families in *Pneumocystis*.

843 Fig. S8. Evolutionary history of CFEM domains in *Pneumocystis*.

844 Fig. S9. Evolutionary history of introns in *Pneumocystis* and Taphrinomycotina fungi.

845 Fig. S10. RAxML phylogeny and phylogenic networks of Msg genes.

846 Fig. S11. Phylodating of major surface glycoproteins in *Pneumocystis.*

847 Table S1. Clinical information and demographic data of individual samples.

848 Table S2. Statistics and a posteriori classification of reads used in this study.

849 Table S3. Statistics of different *Pneumocystis* genome assemblies.

850 Table S4. Genome rearrangements among different *Pneumocystis* species.

851 Table S5. Pairwise nucleotide divergence (%) among *Pneumocystis* genomes.

852 Table S6. Subtelomeres in *P. macacae*

853 Table S7. *P. jirovecii* genome-wide signatures of selection.

854

855 **Acknowledgments:**

856 **Funding:** This work has been funded in whole or in part with federal funds from the

857 Intramural Research Program of the US National Institutes of Health (NIH) Clinical

858 Center and the National Institute of Allergy and Infectious Diseases (NIAID). This study

859 used the Office of Cyber Infrastructure and Computational Biology (OCICB) High

860 Performance Computing (HPC) cluster at the National Institute of Allergy and Infectious

861 Diseases (NIAID), Bethesda, MD. This study also utilized the high-performance

862 computational capabilities of the Biowulf Linux cluster at the National Institutes of
863 Health, Bethesda, MD (http://biowulf.nih.gov). **Author contributions:** O.H.C, L.M and
864 J.A.K conceived the project and designed all the experiments. L.M, O.H.C, C.W.L, J.B,
865 J.X, J.S, R.B, B.P, K.V.R, R.K, A.S, M.C, V.H, J.C, L.P, M.T.C, G.K, Y.L, J.A.K
866 performed the laboratory work to obtain samples for sequencing. O.H.C, L.M, J.P.D,
867 P.P.K, J.L developed and implemented methods for sample processing, library
868 preparation and sequencing. O.H.C, L.M, J.E.S, C.A.C, N.S.U analyzed the data. O.H.C,
869 L.M and J.A.K drafted the manuscript, which was revised by all authors. J.E.S. and
870 C.A.C. are CIFAR Fellows in the program Fungal Kingdom: Threats and Opportunities.
871 **Competing interests:** The authors declare no competing financial interest. **Data and**
872 **materials availability:** All data needed to evaluate the conclusions in the paper are
873 present in the paper and/or the Supplementary Materials.
874
875
876 The content of this publication does not necessarily reflect the views or policies of the
877 Department of Health and Human Services, nor does mention of trade names,
878 commercial products, or organizations imply endorsement by the U.S. Government.
879
880
881
882
883
884
885

886 **Figures:**

887 **Fig. 1. Whole genome structure and synteny among *Pneumocystis* species.** Species
888 names and their genome assembly identifiers are shown on the left. Horizontal
889 black lines on the right represent sequences of all scaffolds for each genome laid
890 end-to-end, with their nucleotide positions indicated at the bottom. Dark thick
891 squares represent short scaffolds. Syntenic regions between genomes are linked
892 with vertical gray lines. Reference genome assemblies of *P. jirovecii*, *P. carinii*
893 and *P. murina* are from a prior study (*13*).

894

895 **Fig. 2. Phylogeny and divergence times of *Pneumocystis* species.** a, Maximum
896 likelihood phylogeny constructed using 106 single-copy genes based on 1,000
897 replicates from 24 annotated fungal genome assemblies including 9 from
898 *Pneumocystis* (highlighted with green background). Only one assembly is shown
899 for each species except there are three for *P. canis* (assemblies Ck1, Ck2 and A).
900 Bootstrap support (%) is presented on the branches. The fungal major
901 phylogenetic phyla and subphyla are represented by their initials: *As*
902 (Ascomycota), *Ba* (Basidiomycota), *Pe* (Pezizomycotina), *Mu* (Mucoromycota)
903 and *Ta* (Taphrinomycotina). b, Schematic representation of species phylogeny
904 and association between *Pneumocystis* species and their respective mammalian
905 hosts. The dashed arrows directed lines represent the specific parasite-host
906 relationships. c, Divergence times of *Pneumocystis* species and mammals.
907 Divergence time medians are represented as squares for hosts and as circles for
908 *Pneumocystis*, and the horizontal lines represent the 95% confidence intervals

(CI), which are color-coded the same for each *Pneumocystis* and its host. Closed elements represent nodes that are significantly different in term of divergence times (non-overlapping confidence intervals) whereas open elements represent nodes with overlapping confidence intervals. Catarrhini, taxonomic category (parvorder) including Humans, great apes, gibbons and Old-World monkeys. Euarchontoglires, superorder of mammals including rodents, lagomorphs, treeshrews, colugos and primates. Glires, taxonomic clade consisting of rodents and lagomorphs. Laurasiatheria, taxonomic clade of placental mammals that includes shrews, whales, bats, and carnivorans. Mya, million years ago. K-Pg, Cretaceous-Paleogene. The dotted vertical line representing the K-Pg mass extinction event at 66 mya is included for context only.

**Fig. 3. Distribution of protein families among *Pneumocystis* species.** a, Heatmap of Pfam protein domains with significant differences (Wilcoxon signed-rank test, $p < 0.05$) are included if the domain appears at least once in the following comparisons: primate *Pneumocystis* (*P. jirovecii* and *P. macacae*) versus other *Pneumocystis*, clade P1 (*P. jirovecii*, *P. macacae*, *P. oryctolagi*, *P. canis* Ck1) versus clade P2 (*P. carinii*, *P. murina* and *P. wakefieldiae*), primate *Pneumocystis* versus clade P2. The number of proteins containing each domain is indicated within each cell for each species. The heat map is colored according to a score, as indicated by the key at the upper right corner. b, Heatmap of distribution of enzymes (represented by Enzyme Commission numbers), with their presence and absence indicated by black and grey colored cells, respectively.

**Fig. 4. Clustering of *Pneumocystis* major surface glycoproteins (Msg).** a, Graphical representation of similarity between 482 Msg proteins from 7 *Pneumocystis* species generated using the Fruchterman Reingold algorithm. A 3-D model of a representative Msg protein A1 family (NCBI accession number T551_00910) generated using DESTINI is presented in the upper left insert. Individual protein sequences are shown as dots and color-coded by species as shown at the bottom. The edge between two dots indicates a global pairwise identity equal or greater than 45%. The letters represent Msg families (A to E) and subfamilies (A1 to A3). N and U letters represent potentially novel Msg sequences (relative to our prior study (*41*)) and unclassified sequences, respectively. For sake of clarity only the major clusters were annotated. b, Phylogenetic network of a subset of Msg family A1 ($n$ = 97) in primate *Pneumocystis* including *P. jirovecii* (red) and *P. macacae* (dark cyan) suggesting recombination events at the root of the network. Nodes with more than two parents represent reticulate events. Bar represent the number of amino acids substitution per site. c, Phylogenetic network of Msg family A1 ($n$ = 33) in *P. oryctolagi* (red violet) and *P. canis* (light blue). d, Phylogenetic network of Msg family A1 ($n$ = 113) in rodent *Pneumocystis* including *P. carinii* (green), *P. murina* (dark blue) and *P. wakefieldiae* (blue violet). The complete phylogenetic network is provided in Supplementary Data.

**Fig. 5. Evolution of Msg cysteine-rich protein domains in *Pneumocystis*.** a, Heatmap showing the distribution of Msg domains in each *Pneumocystis* species. The color

955 change from blue- orange-brown indicates an increase in the number of domains.
956 b, Graphical representation of protein similarity between domains, which
957 highlights that the domains were present in the most recent common ancester and
958 were maintained other than perhaps domains M1 and M3. Domains are clustered
959 by a minimum BLASTp cutoff of 70% protein identity. c, Maximum likelihood
960 tree of the M1 domain. In both panels b and c, domains are color-coded by
961 species as shown at the bottom.

962

963 **Fig. 6. Overview of the genomic evolution of the *Pneumocystis* genus.** Gene families
964 are represented by letters: A to E for the five families of major surface
965 glycoproteins (Msg) with the A family being further subdivided into three
966 subfamilies A1, A2, and A3; K and R for kexins and arginine-glycine rich
967 proteins, respectively. Larger fonts indicate expansions as inferred by maximum
968 likelihood phylogenetic trees and networks. Dashed lines represent ancient
969 hybridization between *P. carinii* and *P. wakefieldiae*. Detailed analysis also
970 reveals distinct phylogenetic clusters within subfamilies. Introns and CFEM
971 (common in fungal extracellular membrane) domains are enriched in
972 *Pneumocystis* genes which indicate that these elements were likely present in the
973 most recent common ancestor of *Pneumocystis* species. Animal icons were
974 obtained from http://phylopic.org.

975

976 **References**

977 1. I. Durand-Joly *et al.*, Pneumocystis carinii f. sp. hominis is not infectious for
978 SCID mice. *J Clin Microbiol* **40**, 1862-1865 (2002).
979 2. F. Gigliotti, A. G. Harmsen, C. G. Haidaris, P. J. Haidaris, Pneumocystis carinii is
980 not universally transmissible between mammalian species. *Infect Immun* **61**,
981 2886-2890 (1993).
982 3. M. T. Cushion, S. P. Keely, J. R. Stringer, Molecular and phenotypic description
983 of Pneumocystis wakefieldiae sp. nov., a new species in rats. *Mycologia* **96**, 429-
984 438 (2004).
985 4. S. P. Keely, J. M. Fischer, J. R. Stringer, Evolution and speciation of
986 Pneumocystis. *J Eukaryot Microbiol* **50 Suppl**, 624-626 (2003).
987 5. O. H. Cisse *et al.*, Comparative Population Genomics Analysis of the Mammalian
988 Fungal Pathogen Pneumocystis. *MBio* **9**, e00381-00318 (2018).
989 6. N. S. Upham, J. A. Esselstyn, W. Jetz, Inferring the mammal tree: Species-level
990 sets of phylogenies for questions in ecology, evolution, and conservation. *PLoS*
991 *Biol* **17**, e3000494 (2019).
992 7. I. McDougall, F. H. Brown, J. G. Fleagle, Stratigraphic placement and age of
993 modern humans from Kibish, Ethiopia. *Nature* **433**, 733-736 (2005).
994 8. Y. Suzuki, M. Tomozawa, Y. Koizumi, K. Tsuchiya, H. Suzuki, Estimating the
995 molecular evolutionary rates of mitochondrial genes referring to Quaternary ice
996 age events with inferred population expansions and dispersals in Japanese
997 Apodemus. *BMC Evol Biol* **15**, 187 (2015).
998 9. J. Guillot *et al.*, Parallel phylogenies of Pneumocystis species and their
999 mammalian hosts. *J Eukaryot Microbiol* **Suppl**, 113S-115S (2001).

10. A. Latinne *et al.*, Genetic diversity and evolution of Pneumocystis fungi infecting wild Southeast Asian murid rodents. *Parasitology* **145**, 885-900 (2018).

11. J. Petruzela *et al.*, Evolutionary history of Pneumocystis fungi in their African rodent hosts. *Infect Genet Evol* **75**, 103934 (2019).

12. O. H. Cisse, M. Pagni, P. M. Hauser, De novo assembly of the Pneumocystis jirovecii genome from a single bronchoalveolar lavage fluid specimen from a patient. *MBio* **4**, e00428-00412 (2012).

13. L. Ma *et al.*, Genome analysis of three Pneumocystis species reveals adaptation mechanisms to life exclusively in mammalian hosts. *Nat Commun* **7**, 10740 (2016).

14. B. E. Slaven *et al.*, Draft assembly and annotation of the Pneumocystis carinii genome. *J Eukaryot Microbiol* **53 Suppl 1**, S89-91 (2006).

15. B. Lundgren, R. Cotton, J. D. Lundgren, J. C. Edman, J. A. Kovacs, Identification of Pneumocystis carinii chromosomes and mapping of five genes. *Infect Immun* **58**, 1705-1710 (1990).

16. A. P. Underwood, E. J. Louis, R. H. Borts, J. R. Stringer, A. E. Wakefield, Pneumocystis carinii telomere repeats are composed of TTAGGG and the subtelomeric sequence contains a gene encoding the major surface glycoprotein. *Mol Microbiol* **19**, 273-281 (1996).

17. L. Ma *et al.*, Sequencing and characterization of the complete mitochondrial genomes of three Pneumocystis species provide new insights into divergence between human and rodent Pneumocystis. *Faseb J* **27**, 1962-1972 (2013).

1022 18. H. Shimodaira, M. Hasegawa, Multiple comparisons of log-likelihoods with
1023 applications to phylogenetic inference. *Mol Biol Evol* **16**, 1114-1116 (1999).
1024 19. C. M. Aliouat-Denis *et al.*, Pneumocystis species, co-evolution and pathogenic
1025 power. *Infect Genet Evol* **8**, 708-726 (2008).
1026 20. Y. Kitazoe *et al.*, Robust time estimation reconciles views of the antiquity of
1027 placental mammals. *PLoS One* **2**, e384 (2007).
1028 21. J. L. S. Xing-Xing Shen, Abigail L. LaBella, Dana A. Opulente, Xiaofan Zhou,
1029 Jacek Kominek, Yuanning Li, Marizeth Groenewald, Chris Todd Hittinger,
1030 Antonis Rokas, Genome-scale phylogeny and contrasting modes of genome
1031 evolution in the fungal phylum Ascomycota. *bioRxiv* **05**, 088658 (2020).
1032 22. S. M. Kielbasa, R. Wan, K. Sato, P. Horton, M. C. Frith, Adaptive seeds tame
1033 genomic sequence comparison. *Genome Res* **21**, 487-493 (2011).
1034 23. T. S. Korneliussen, A. Albrechtsen, R. Nielsen, ANGSD: Analysis of Next
1035 Generation Sequencing Data. *BMC Bioinformatics* **15**, 356 (2014).
1036 24. A. E. McBride, A. K. Conboy, S. P. Brown, C. Ariyachet, K. L. Rutledge,
1037 Specific sequences within arginine-glycine-rich domains affect mRNA-binding
1038 protein function. *Nucleic Acids Res* **37**, 4322-4330 (2009).
1039 25. D. A. Russian *et al.*, Characterization of a multicopy family of genes encoding a
1040 surface-expressed serine endoprotease in rat Pneumocystis carinii. *Proc Assoc Am*
1041 *Physicians* **111**, 347-356 (1999).
1042 26. G. Bairwa, W. Hee Jung, J. W. Kronstad, Iron acquisition in fungal pathogens of
1043 humans. *Metallomics* **9**, 215-227 (2017).

1044 27. T. Tanaka, Y. Tateno, T. Gojobori, Evolution of vitamin B6 (pyridoxine)
1045 metabolism by gain and loss of genes. *Mol Biol Evol* **22**, 243-250 (2005).
1046 28. C. Gournas, M. Prevost, E. M. Krammer, B. Andre, Function and Regulation of
1047 Fungal Amino Acid Transporters: Insights from Predicted Structure. *Adv Exp*
1048 *Med Biol* **892**, 69-106 (2016).
1049 29. G. Y. Lipschik, H. Masur, J. A. Kovacs, Polyamine metabolism in Pneumocystis
1050 carinii. *J Infect Dis* **163**, 1121-1127 (1991).
1051 30. I. Velasco, S. Tenreiro, I. L. Calderon, B. Andre, Saccharomyces cerevisiae Aqr1
1052 is an internal-membrane transporter involved in excretion of amino acids.
1053 *Eukaryot Cell* **3**, 1492-1503 (2004).
1054 31. J. E. Stajich, F. S. Dietrich, S. W. Roy, Comparative genomic analysis of fungal
1055 genomes reveals intron-rich ancestors. *Genome Biol* **8**, R223 (2007).
1056 32. O. H. Cisse *et al.*, Genome sequencing of the plant pathogen Taphrina deformans,
1057 the causal agent of peach leaf curl. *MBio* **4**, e00055-00013 (2013).
1058 33. Y. Yu, L. Nakhleh, A maximum pseudo-likelihood approach for phylogenetic
1059 networks. *BMC Genomics* **16 Suppl 10**, S10 (2015).
1060 34. E. Mazars *et al.*, Isoenzyme diversity in Pneumocystis carinii from rats, mice, and
1061 rabbits. *J Infect Dis* **175**, 655-660 (1997).
1062 35. T. Aghova *et al.*, Fossils know it best: Using a new set of fossil calibrations to
1063 improve the temporal phylogenetic framework of murid rodents (Rodentia:
1064 Muridae). *Mol Phylogenet Evol* **128**, 98-111 (2018).
1065 36. S. B. Araujo *et al.*, Understanding Host-Switching by Ecological Fitting. *PLoS*
1066 *One* **10**, e0139225 (2015).

1067 37. S. Restrepo, J. F. Tabima, M. F. Mideros, N. J. Grunwald, D. R. Matute,
1068 Speciation in fungal and oomycete plant pathogens. *Annu Rev Phytopathol* **52**,
1069 289-316 (2014).
1070 38. C. R. Icenhour, J. Arnold, M. Medvedovic, M. T. Cushion, Competitive
1071 coexistence of two Pneumocystis species. *Infect Genet Evol* **6**, 177-186 (2006).
1072 39. J. Zhang, R. Nielsen, Z. Yang, Evaluation of an improved branch-site likelihood
1073 method for detecting positive selection at the molecular level. *Mol Biol Evol* **22**,
1074 2472-2479 (2005).
1075 40. E. Schmid-Siegert *et al.*, Mechanisms of Surface Antigenic Variation in the
1076 Human Pathogenic Fungus Pneumocystis jirovecii. *MBio* **8**, e01470-01417
1077 (2017).
1078 41. L. Ma *et al.*, Diversity and Complexity of the Large Surface Protein Family in the
1079 Compacted Genomes of Multiple Pneumocystis Species. *mBio* **11**, (2020).
1080 42. K. B. R. Morand S., Poulin R., *Micromammals and Macroparasites*. (2006).
1081 43. M. T. Cushion *et al.*, Transcriptome of Pneumocystis carinii during fulminate
1082 infection: carbohydrate metabolism and the concept of a compatible parasite.
1083 *PLoS One* **2**, e423 (2007).
1084 44. O. H. Cisse, M. Pagni, P. M. Hauser, Comparative Genomics Suggests That the
1085 Human Pathogenic Fungus Pneumocystis jirovecii Acquired Obligate Biotrophy
1086 through Gene Loss. *Genome Biology and Evolution* **6**, 1938-1948 (2014).
1087 45. A. M. Bolger, M. Lohse, B. Usadel, Trimmomatic: a flexible trimmer for Illumina
1088 sequence data. *Bioinformatics* **30**, 2114-2120 (2014).

1089 46. B. Langmead, S. L. Salzberg, Fast gapped-read alignment with Bowtie 2. *Nat*
1090 *Methods* **9**, 357-359 (2012).
1091 47. A. Bankevich *et al.*, SPAdes: a new genome assembly algorithm and its
1092 applications to single-cell sequencing. *J Comput Biol* **19**, 455-477 (2012).
1093 48. F. A. Simao, R. M. Waterhouse, P. Ioannidis, E. V. Kriventseva, E. M. Zdobnov,
1094 BUSCO: assessing genome assembly and annotation completeness with single-
1095 copy orthologs. *Bioinformatics* **31**, 3210-3212 (2015).
1096 49. O. H. Cisse, J. E. Stajich, FGMP: assessing fungal genome completeness. *BMC*
1097 *Bioinformatics* **20**, 184 (2019).
1098 50. G. Parra, K. Bradnam, I. Korf, CEGMA: a pipeline to accurately annotate core
1099 genes in eukaryotic genomes. *Bioinformatics* **23**, 1061-1067 (2007).
1100 51. H. Li, Minimap2: pairwise alignment for nucleotide sequences. *Bioinformatics*
1101 **34**, 3094-3100 (2018).
1102 52. F. J. Sedlazeck *et al.*, Accurate detection of complex structural variations using
1103 single-molecule sequencing. *Nat Methods* **15**, 461-468 (2018).
1104 53. S. Koren *et al.*, Canu: scalable and accurate long-read assembly via adaptive k-
1105 mer weighting and repeat separation. *Genome Res* **27**, 722-736 (2017).
1106 54. R. Vaser, I. Sovic, N. Nagarajan, M. Sikic, Fast and accurate de novo genome
1107 assembly from long uncorrected reads. *Genome Res* **27**, 737-746 (2017).
1108 55. B. J. Walker *et al.*, Pilon: an integrated tool for comprehensive microbial variant
1109 detection and genome assembly improvement. *PLoS One* **9**, e112963 (2014).
1110 56. H. Li, Aligning sequence reads, clone sequences and assembly contigs with
1111 BWA-MEM. *arXiv*, 1303.3997 (2013).

1112 57. M. Pertea, D. Kim, G. M. Pertea, J. T. Leek, S. L. Salzberg, Transcript-level
1113 expression analysis of RNA-Seq experiments with HISAT, StringTie and
1114 Ballgown. *Nat Protoc* **11**, 1650-1667 (2016).
1115 58. H. Li *et al.*, The Sequence Alignment/Map format and SAMtools. *Bioinformatics*
1116 **25**, 2078-2079 (2009).
1117 59. M. G. Grabherr *et al.*, Full-length transcriptome assembly from RNA-Seq data
1118 without a reference genome. *Nat Biotechnol* **29**, 644-652 (2011).
1119 60. N. L. Bray, H. Pimentel, P. Melsted, L. Pachter, Near-optimal probabilistic RNA-
1120 Seq quantification. *Nat Biotechnol* **34**, 525-527 (2016).
1121 61. S. AFA, RepeatMasker. (1996-2005).
1122 62. W. Bao, K. K. Kojima, O. Kohany, Repbase Update, a database of repetitive
1123 elements in eukaryotic genomes. *Mob DNA* **6**, 11 (2015).
1124 63. M. G. Grabherr *et al.*, Genome-wide synteny through highly sensitive sequence
1125 alignment: Satsuma. *Bioinformatics* **26**, 1145-1151 (2010).
1126 64. T. UniProt Consortium, UniProt: the universal protein knowledgebase. *Nucleic*
1127 *Acids Res* **46**, 2699 (2018).
1128 65. M. Stanke, S. Waack, Gene prediction with a hidden Markov model and a new
1129 intron submodel. *Bioinformatics* **19 Suppl 2**, ii215-225 (2003).
1130 66. V. Ter-Hovhannisyan, A. Lomsadze, Y. O. Chernoff, M. Borodovsky, Gene
1131 prediction in novel fungal genomes using an ab initio algorithm with
1132 unsupervised training. *Genome Res* **18**, 1979-1990 (2008).

1133 67. B. J. Haas *et al.*, Automated eukaryotic gene structure annotation using
1134 EVidenceModeler and the Program to Assemble Spliced Alignments. *Genome*
1135 *Biol* **9**, R7 (2008).
1136 68. I. J. Tsai *et al.*, Comparative genomics of Taphrina fungi causing varying degrees
1137 of tumorous deformity in plants. *Genome Biol Evol* **6**, 861-872 (2014).
1138 69. C. Holt, M. Yandell, MAKER2: an annotation pipeline and genome-database
1139 management tool for second-generation genome projects. *BMC Bioinformatics*
1140 **12**, 491 (2011).
1141 70. I. Korf, Gene finding in novel genomes. *BMC Bioinformatics* **5**, 59 (2004).
1142 71. P. M. Hauser *et al.*, Comparative Genomics Suggests that the Fungal Pathogen
1143 Pneumocystis Is an Obligate Parasite Scavenging Amino Acids from Its Host's
1144 Lungs. *Plos One* **5**, (2010).
1145 72. A. Pierleoni, P. L. Martelli, R. Casadio, PredGPI: a GPI-anchor predictor. *BMC*
1146 *Bioinformatics* **9**, 392 (2008).
1147 73. B. Eisenhaber, G. Schneider, M. Wildpaner, F. Eisenhaber, A sensitive predictor
1148 for potential GPI lipid modification sites in fungal protein sequences and its
1149 application to genome-wide studies for Aspergillus nidulans, Candida albicans,
1150 Neurospora crassa, Saccharomyces cerevisiae and Schizosaccharomyces pombe. *J*
1151 *Mol Biol* **337**, 243-253 (2004).
1152 74. N. Fankhauser, P. Maser, Identification of GPI anchor attachment signals by a
1153 Kohonen self-organizing map. *Bioinformatics* **21**, 1846-1852 (2005).
1154 75. J. J. Almagro Armenteros *et al.*, SignalP 5.0 improves signal peptide predictions
1155 using deep neural networks. *Nat Biotechnol* **37**, 420-423 (2019).

1156 76. K. H. a. W. Stoffel, TMbase - A database of membrane spanning proteins
1157 segments. *Biol. Chem. Hoppe-Seyler* **374**, 166 (1993).
1158 77. S. El-Gebali *et al.*, The Pfam protein families database in 2019. *Nucleic Acids Res*
1159 **47**, D427-D432 (2019).
1160 78. H. Fang, dcGOR: an R package for analysing ontologies and protein domain
1161 annotations. *PLoS Comput Biol* **10**, e1003929 (2014).
1162 79. C. Claudel-Renard, C. Chevalet, T. Faraut, D. Kahn, Enzyme-specific profiles for
1163 genome annotation: PRIAM. *Nucleic Acids Res* **31**, 6633-6639 (2003).
1164 80. M. Gao, H. Zhou, J. Skolnick, DESTINI: A deep-learning approach to contact-
1165 driven protein structure prediction. *Sci Rep* **9**, 3514 (2019).
1166 81. M. C. Frith, L. Noe, Improved search heuristics find 20,000 new alignments
1167 between human and mouse genomes. *Nucleic Acids Res* **42**, e59 (2014).
1168 82. G. Tesler, GRIMM: genome rearrangements web server. *Bioinformatics* **18**, 492-
1169 493 (2002).
1170 83. A. E. Darling, B. Mau, N. T. Perna, progressiveMauve: multiple genome
1171 alignment with gene gain, loss and rearrangement. *PLoS One* **5**, e11147 (2010).
1172 84. C. Baudet *et al.*, Cassis: detection of genomic rearrangement breakpoints.
1173 *Bioinformatics* **26**, 1897-1898 (2010).
1174 85. A. R. Quinlan, BEDTools: The Swiss-Army Tool for Genome Feature Analysis.
1175 *Curr Protoc Bioinformatics* **47**, 11 12 11-34 (2014).
1176 86. R. A. Farrer, Synima: a Synteny imaging tool for annotated genome assemblies.
1177 *BMC Bioinformatics* **18**, 507 (2017).

1178 87. P. Rice, I. Longden, A. Bleasby, EMBOSS: the European Molecular Biology
1179 Open Software Suite. *Trends Genet* **16**, 276-277 (2000).
1180 88. S. F. Altschul *et al.*, Gapped BLAST and PSI-BLAST: a new generation of
1181 protein database search programs. *Nucleic Acids Res* **25**, 3389-3402 (1997).
1182 89. H. S. Bastian M., Jacomy M, paper presented at the International AAAI
1183 Conference on Weblogs and Social Media, 2009.
1184 90. S. Seton Bocco, M. Csuros, Splice Sites Seldom Slide: Intron Evolution in
1185 Oomycetes. *Genome Biol Evol* **8**, 2340-2350 (2016).
1186 91. M. Csuros, Malin: maximum likelihood analysis of intron evolution in
1187 eukaryotes. *Bioinformatics* **24**, 1538-1539 (2008).
1188 92. D. M. Emms, S. Kelly, OrthoFinder: solving fundamental biases in whole genome
1189 comparisons dramatically improves orthogroup inference accuracy. *Genome Biol*
1190 **16**, 157 (2015).
1191 93. A. Stamatakis, RAxML version 8: a tool for phylogenetic analysis and post-
1192 analysis of large phylogenies. *Bioinformatics* **30**, 1312-1313 (2014).
1193 94. S. Q. Le, O. Gascuel, An improved general amino acid replacement matrix. *Mol*
1194 *Biol Evol* **25**, 1307-1320 (2008).
1195 95. B. Q. Minh *et al.*, IQ-TREE 2: New Models and Efficient Methods for
1196 Phylogenetic Inference in the Genomic Era. *Mol Biol Evol* **37**, 1530-1534 (2020).
1197 96. F. Sievers, D. G. Higgins, Clustal Omega, accurate alignment of very large
1198 numbers of sequences. *Methods Mol Biol* **1079**, 105-116 (2014).

1199 97. L. T. Nguyen, H. A. Schmidt, A. von Haeseler, B. Q. Minh, IQ-TREE: a fast and
1200 effective stochastic algorithm for estimating maximum-likelihood phylogenies.
1201 *Mol Biol Evol* **32**, 268-274 (2015).
1202 98. T. M. Sesterhenn *et al.*, Sequence and structure of the linear mitochondrial
1203 genome of Pneumocystis carinii. *Mol Genet Genomics* **283**, 63-72 (2010).
1204 99. M. Stolzer *et al.*, Inferring duplications, losses, transfers and incomplete lineage
1205 sorting with nonbinary species trees. *Bioinformatics* **28**, i409-i415 (2012).
1206 100. M. Csuros, Count: evolutionary analysis of phylogenetic profiles with parsimony
1207 and likelihood. *Bioinformatics* **26**, 1910-1912 (2010).
1208 101. D. H. Huson, D. Bryant, Application of phylogenetic networks in evolutionary
1209 studies. *Mol Biol Evol* **23**, 254-267 (2006).
1210 102. G. McGuire, F. Wright, TOPAL 2.0: improved detection of mosaic sequences
1211 within multiple alignments. *Bioinformatics* **16**, 130-134 (2000).
1212 103. V. Ranwez, E. J. P. Douzery, C. Cambon, N. Chantret, F. Delsuc, MACSE v2:
1213 Toolkit for the Alignment of Coding Sequences Accounting for Frameshifts and
1214 Stop Codons. *Mol Biol Evol* **35**, 2582-2584 (2018).
1215 104. R. Bouckaert *et al.*, BEAST 2: a software platform for Bayesian evolutionary
1216 analysis. *PLoS Comput Biol* **10**, e1003537 (2014).
1217 105. A. J. Drummond, S. Y. Ho, M. J. Phillips, A. Rambaut, Relaxed phylogenetics
1218 and dating with confidence. *PLoS Biol* **4**, e88 (2006).
1219 106. T. Gernhard, The conditioned reconstructed process. *J Theor Biol* **253**, 769-778
1220 (2008).

1221 107. J. Heled, A. J. Drummond, Calibrated birth-death phylogenetic time-tree priors
1222 for bayesian inference. *Syst Biol* **64**, 369-383 (2015).
1223 108. M. Hasegawa, H. Kishino, T. Yano, Dating of the human-ape splitting by a
1224 molecular clock of mitochondrial DNA. *J Mol Evol* **22**, 160-174 (1985).
1225 109. C. Beimforde *et al.*, Estimating the Phanerozoic history of the Ascomycota
1226 lineages: combining fossil and molecular data. *Mol Phylogenet Evol* **78**, 386-398
1227 (2014).
1228 110. R. Lanfear, P. B. Frandsen, A. M. Wright, T. Senfeld, B. Calcott, PartitionFinder
1229 2: New Methods for Selecting Partitioned Models of Evolution for Molecular and
1230 Morphological Phylogenetic Analyses. *Mol Biol Evol* **34**, 772-773 (2017).
1231 111. T. S. Korneliussen, I. Moltke, A. Albrechtsen, R. Nielsen, Calculation of Tajima's
1232 D and other neutrality test statistics from low depth next-generation sequencing
1233 data. *BMC Bioinformatics* **14**, 289 (2013).
1234 112. M. Fumagalli *et al.*, Quantifying population genetic differentiation from next-
1235 generation sequencing data. *Genetics* **195**, 979-992 (2013).
1236 113. A. R. Quinlan, I. M. Hall, BEDTools: a flexible suite of utilities for comparing
1237 genomic features. *Bioinformatics* **26**, 841-842 (2010).
1238 114. R. C. Edgar, MUSCLE: multiple sequence alignment with high accuracy and high
1239 throughput. *Nucleic Acids Res* **32**, 1792-1797 (2004).
1240 115. T. C. Bruen, H. Philippe, D. Bryant, A simple and robust statistical test for
1241 detecting the presence of recombination. *Genetics* **172**, 2665-2681 (2006).

116. A. M. Kozlov, D. Darriba, T. Flouri, B. Morel, A. Stamatakis, RAxML-NG: A fast, scalable, and user-friendly tool for maximum likelihood phylogenetic inference. *Bioinformatics*, (2019).

117. D. H. Huson, C. Scornavacca, Dendroscope 3: an interactive tool for rooted phylogenetic trees and networks. *Syst Biol* **61**, 1061-1067 (2012).

118. Z. Yang, PAML 4: phylogenetic analysis by maximum likelihood. *Mol Biol Evol* **24**, 1586-1591 (2007).

119. J. Koster, S. Rahmann, Snakemake--a scalable bioinformatics workflow engine. *Bioinformatics* **28**, 2520-2522 (2012).

120. R. C. Team, in *R Foundation for Statistical Computing*. (Vienna, Austria, 2018).

121. L. G. Bell MA, strap: an R package for plotting phylogenies against stratigraphy and assessing their stratigraphic congruence. *Palaeontology* **58**, 379–389 (2015).

122. G. E. Crooks, G. Hon, J. M. Chandonia, S. E. Brenner, WebLogo: a sequence logo generator. *Genome Res* **14**, 1188-1190 (2004).

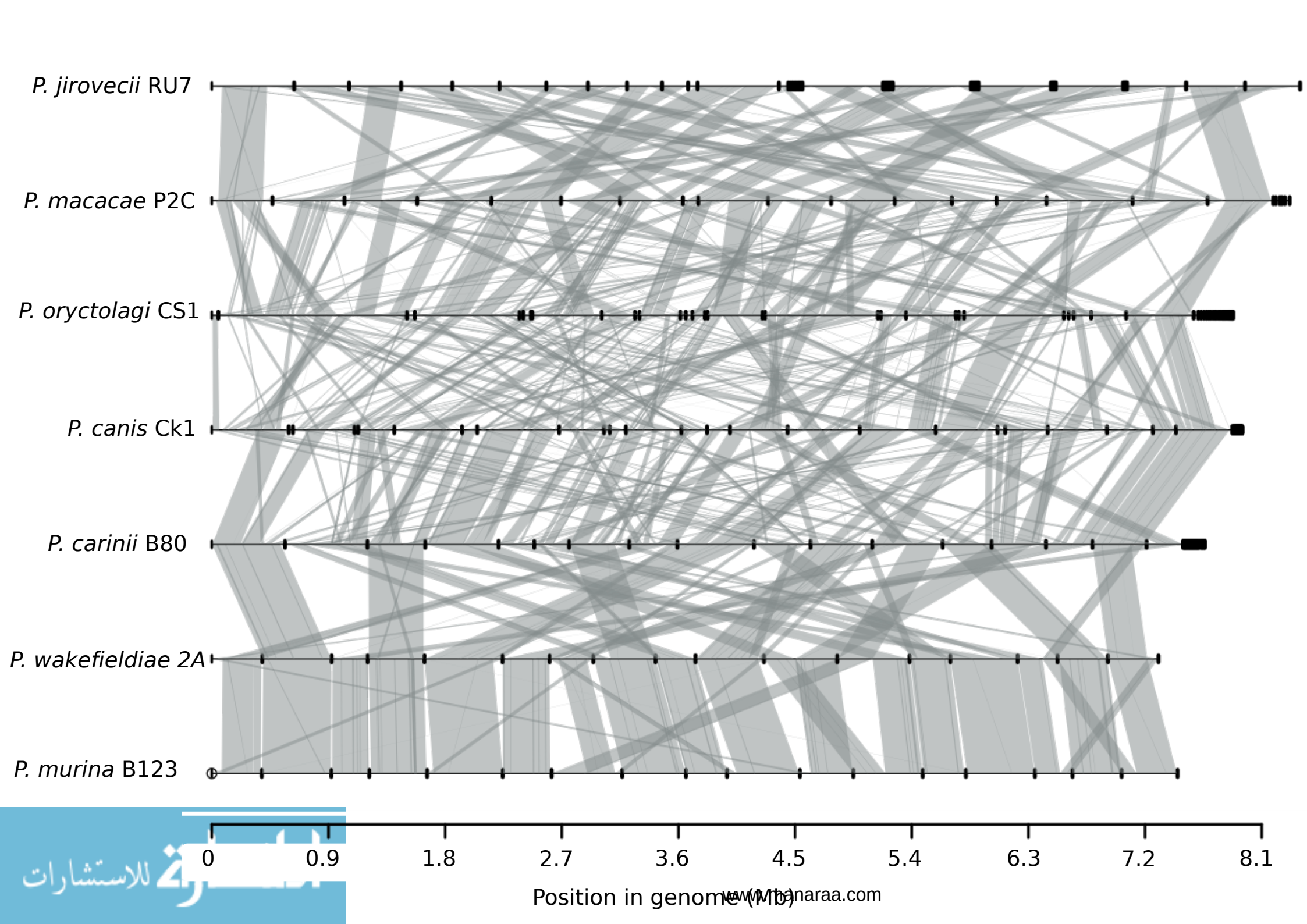

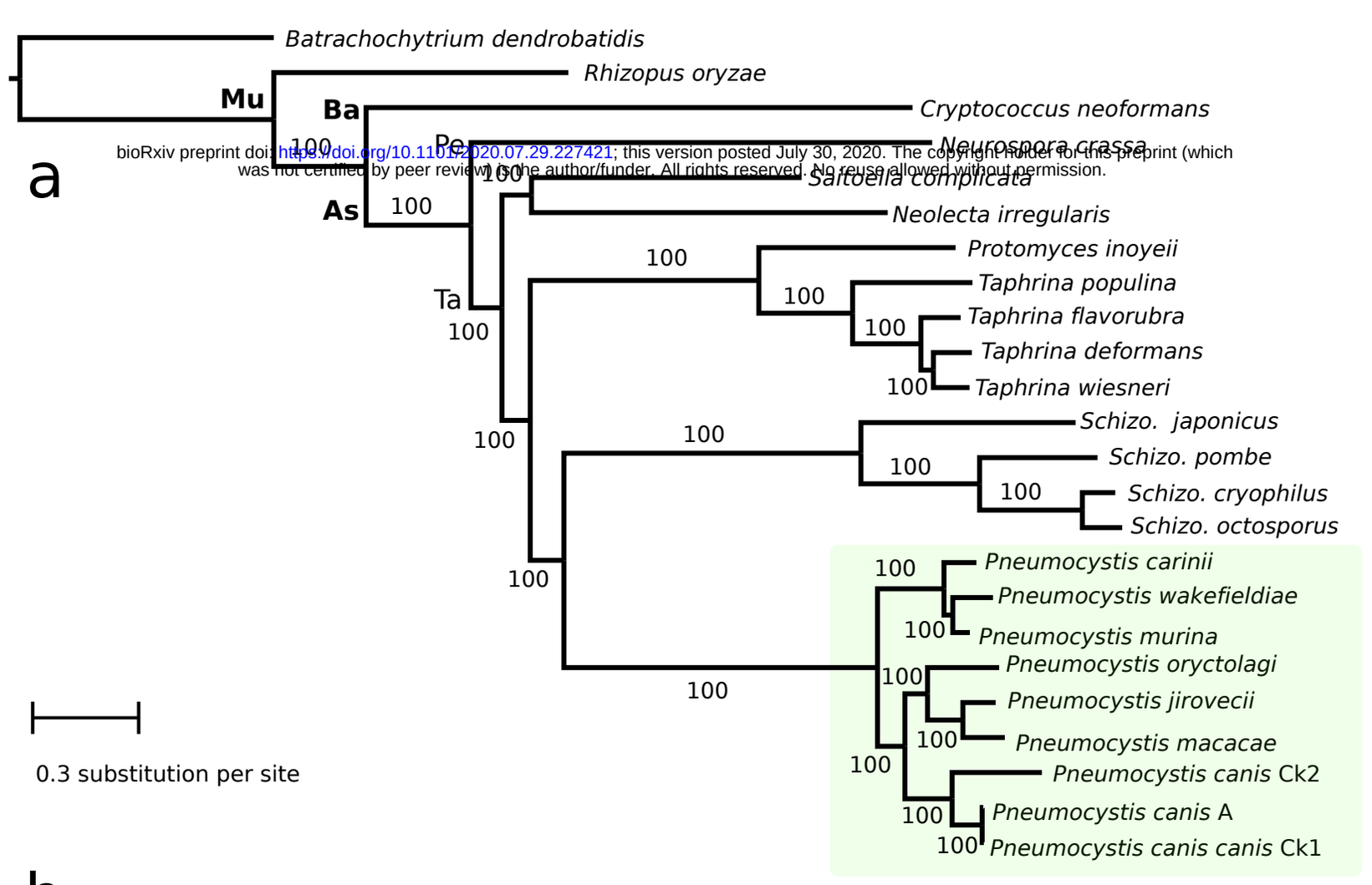


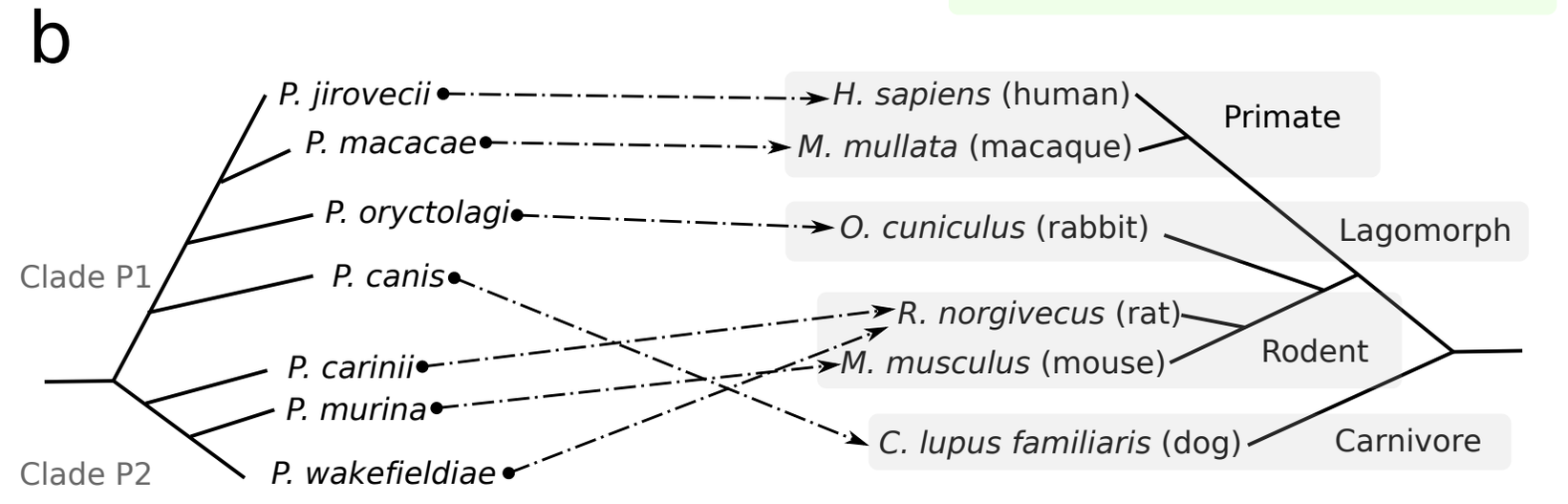


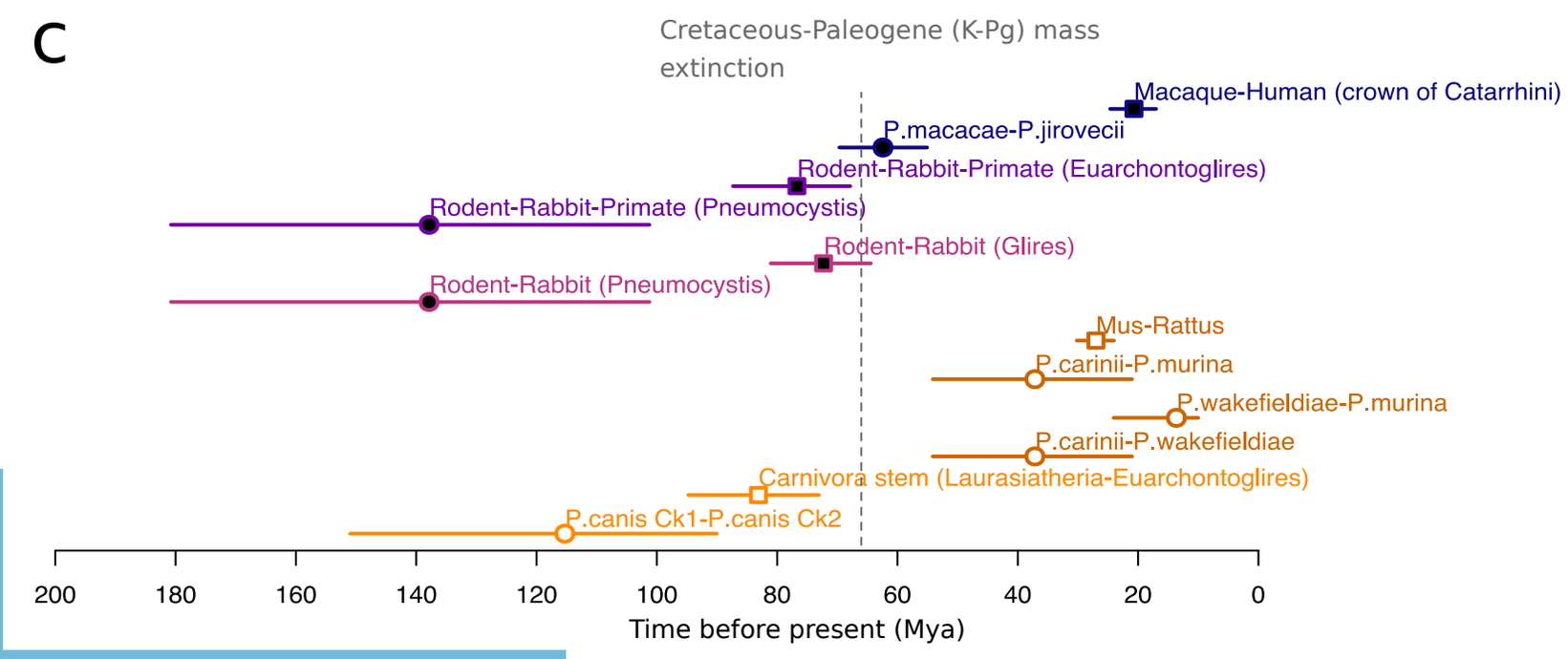

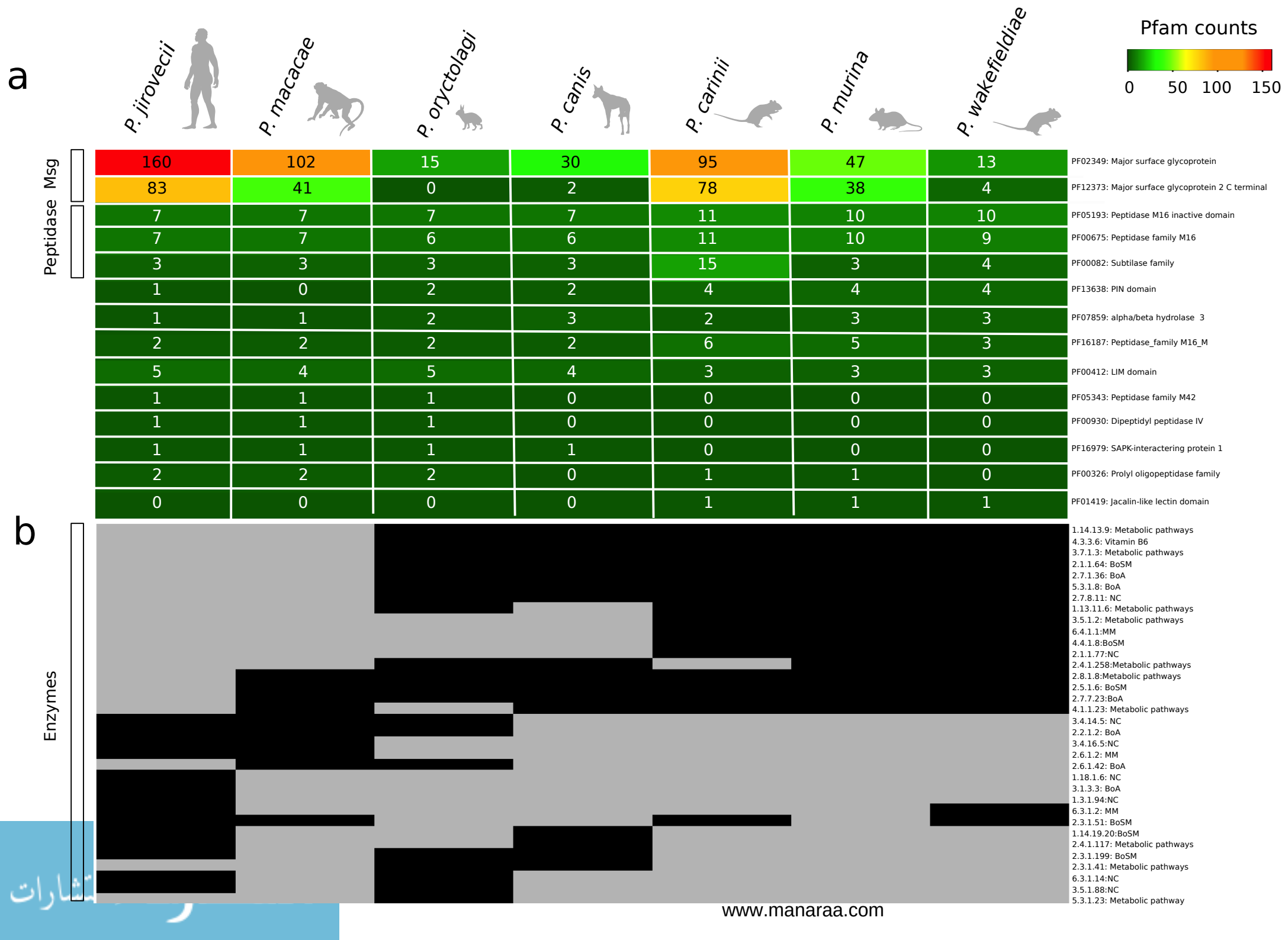

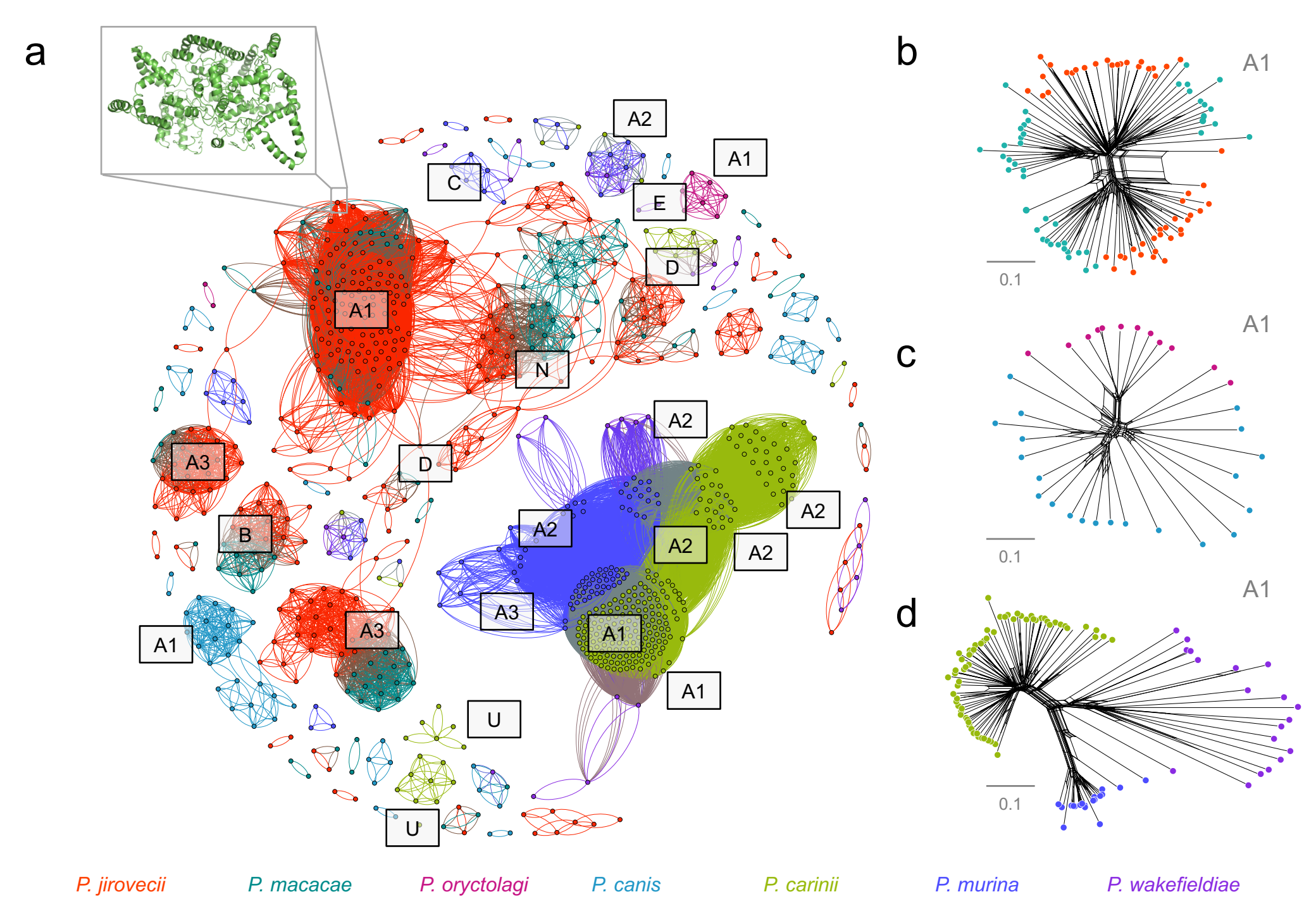
a
A2
A1
C
E
D
A1
N
A3
D
A2
A2
A2
A2
B
A2
A3
A1
A3
A1
A1
U
U
b
A1
0.1
c
A1
0.1
d
A1
0.1
P. jirovecii
P. macacae
P. oryctolagi
P. canis
P. carinii
P. murina
P. wakefieldiae

**a**

| | N1 | M1 | M2 | M3 | M4 | M5 | C1 |
|---|---|---|---|---|---|---|---|
| *P. jirovecii* | 51 | 91 | 83 | 72 | 69 | 64 | 61 |
| *P. macacae* | 46 | 125 | 95 | 64 | 88 | 86 | 87 |
| *P. oryctolagi* | 9 | 16 | 17 | 9 | 5 | 2 | 9 |
| *P. canis* | 5 | 29 | 24 | 19 | 11 | 5 | 20 |
| *P. carinii* | 84 | 65 | 68 | 56 | 57 | 54 | 51 |
| *P. murina* | 54 | 22 | 34 | 19 | 28 | 29 | 24 |
| *P. wakefieldiae* | 12 | 5 | 8 | 2 | 3 | 5 | 5 |

**b**

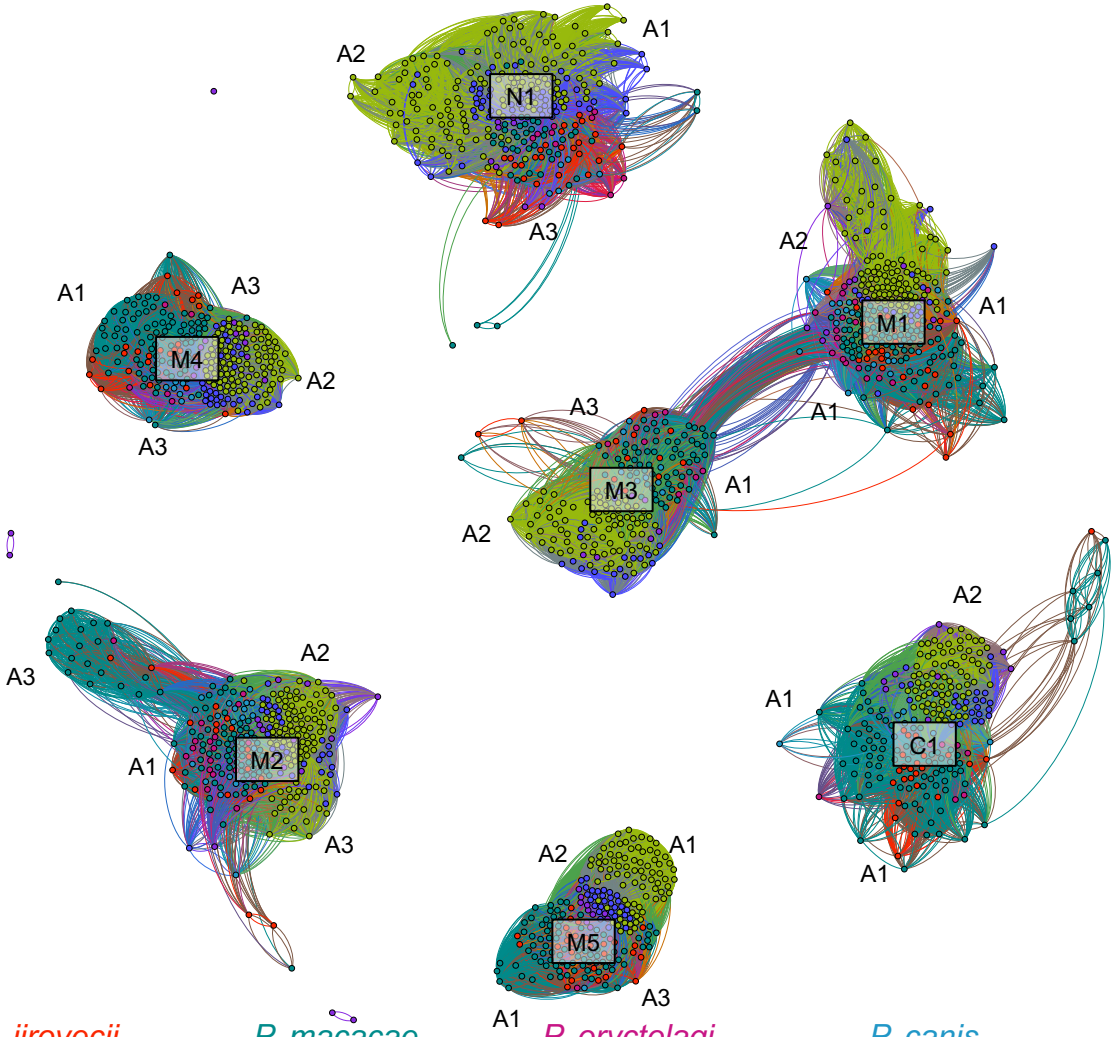


**c**

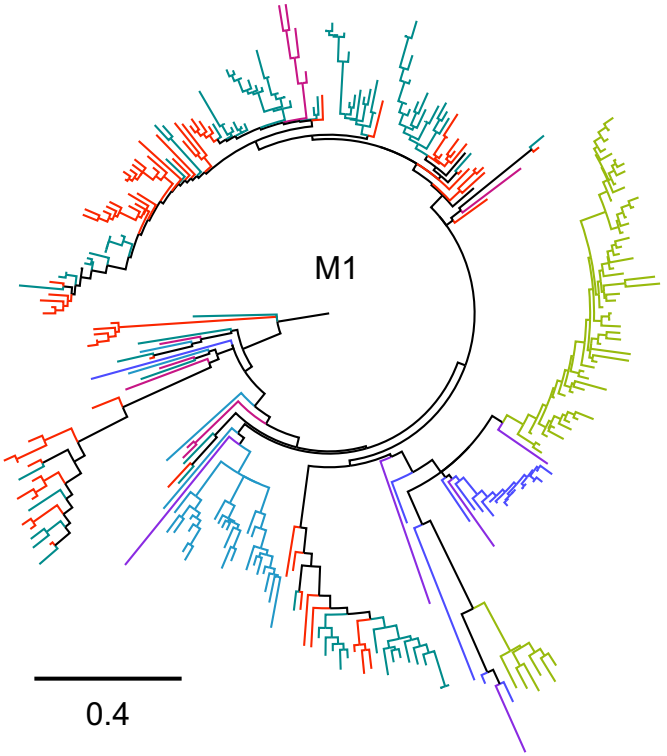


*P. jirovecii* *P. macacae* *P. oryctolagi* *P. canis* *P. carinii* *P. murina* *P. wakefieldiae*

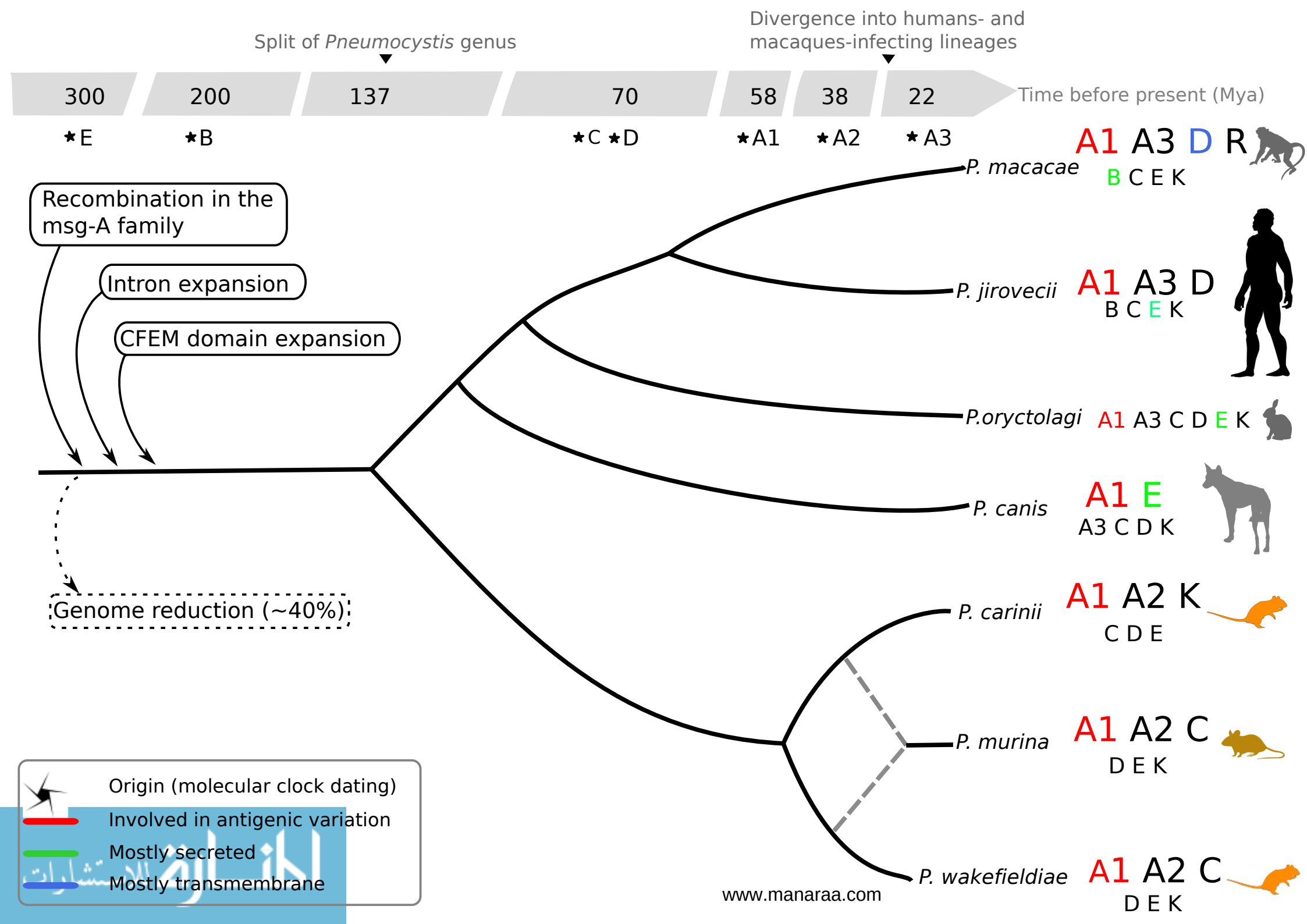
Split of *Pneumocystis* genus
Divergence into humans- and macaques-infecting lineages
300
200
137
70
58
38
22
Time before present (Mya)
★E
★B
★C ★D
★A1
★A2
★A3
Recombination in the msg-A family
Intron expansion
CFEM domain expansion
Genome reduction (~40%)
P. macacae
A1 A3 D R
B C E K
P. jirovecii
A1 A3 D
B C E K
P.oryctolagi
A1 A3 C D E K
P. canis
A1 E
A3 C D K
P. carinii
A1 A2 K
C D E
P. murina
A1 A2 C
D E K
P. wakefieldiae
A1 A2 C
D E K
Origin (molecular clock dating)
Involved in antigenic variation
Mostly secreted
Mostly transmembrane
www.manaraa.com